Development of a lipid-based modular drug-RNA co-delivery nanoparticle approach for breast cancer therapy

Zhiqian Chen

A thesis

submitted in partial fulfillment of the

requirement for the degree of

Master of Science

University of Washington

2025

Committee:

Rodney JY Ho

Qingxin Mu

Program Authorized to Office Degree:

Pharmaceutics

University of Washington

Abstract

Development of a lipid-based modular drug-RNA co-delivery nanoparticle approach for breast cancer therapy

Zhiqian Chen

Chair of the Supervisory Committee:
Rodney JY Ho
Department of Pharmaceutics

Triple-negative breast cancer (TNBC) is a form of breast cancer characterized by the low expression of hormone and HER2 receptors, leading to the ineffectiveness of receptor-targeted drug treatments. While receptor independent chemotherapeutic drugs, when used alone has been ineffective for TNBC, drug-combination prescribed as standard treatments against TNBC exhibit some impact, but low impact against metastatic breast cancer (MBC). Therapeutic nucleic acid polymers such as mRNA and siRNA could be used to shut-down tumorigenic potential of breast tumor. However, stability of mRNA and siRNA as well as the highly negative charge nucleic acid access across cell membranes are considered key barriers. A carrier that stabilizes and enhances cell penetration will overcome the barrier to make nucleic polymers to inhibit breast

tumor growth. If the carrier can also carry a highly potent chemotherapeutic agent, one can co-delivery and synchronize inhibition of breast cancer cells at multiple check points. Therefore, drug-gene combination nanoparticles have been designed, characterized and explore the synergistic therapeutic effects in breast cancer cells. Lipid-based nanoparticle, which showed good endosomal escape capability, is used as a carrier to carry both nucleic acid molecules and a highly potent chemotherapeutic drug. The overall goal is to optimize multi-targeting ability of both genetic materials and drug, and in doing so with novel carrier, one can overcome biological barriers to gain drug-gene access into cells and thus overcoming drug resistance. In our previous studies, a lipid-based drug combination nanoparticle composed of gemcitabine (GEM or G) and paclitaxel (PTX or T), referred to as GT-in-DcNP was reported to enable synchronized delivery of GT, two chemotherapeutic drugs. In a mouse metastatic tumor model, GT-in-DcNP has demonstrated to inhibit metastatic tumor growth in the lung in a dose-dependent manner with margin of safety. However, GT-in-DcNP structure was not designed for co-formulation with nucleic acid polymers. To enable the loading of RNA nucleic polymeric molecules, we have incorporated positive charge on nanoparticles to both attach and stabilize RNA and coated with additional layer of neutralizing or targeting polymers to enhance cell attachment and delivery. This approach is often referred to as layer-by-layer (LbL) formulation. With a nanoparticle core, a layer of charged polymers, such as negatively charged RNA polymer or positively charged chitosan polymer, could be coated on nanoparticle core through electrostatic interactions between opposite charges. On the outside of first polymer layer, another layer of polymers with opposite charges could be coated, further enhancing the biocompatibility, stability, or targeting according to the specific polymer coated. More than one layer of therapeutic agents could be loaded in LbL formulation approach, which increased the loading capacity of therapeutic agents

in lipid-based nanoparticles. This thesis research leverages on the previously developed GT-in-DcNP. The overarching goal of this study is design and characterize a nanoparticle platform that carries both RNA molecules and highly potent chemotherapeutic drugs, referred to as DG-in-LNP so that a synchronized knock-out of multiple tumorigenic checkpoints within the TNBC without relying on the receptor targets.

In this study, DG-in-LNP core with different formulations were designed, prepared, and characterized. Based on the LbL coating strategies, mRNA or siRNA was stabilized with their electrostatic interactions with positively charged DG-in-LNP core. The final coating included varying concentration of the positively charged, cationic chitosan polymers with a defined molarecular weight.

We validated that the addition of a cationic lipid (DOTAP) added to DG-in-LNP core can provide surface positive charge on the nanoparticles which enable the binding of negatively charged RNA polymers. To further stabilize the nanoparticle structure and RNA molecules, we added cholesterol into the core of lipid nanoparticles. We also studied the impact of solvent effects, and variation on PTX loading regarding nanoparticle stability and surface charge. The composition with the highest stability and optimal size-charge properties, diameter = 111.3 nm and zeta potential +15.6 mV, was used for loading of RNA and chitosan polymer. With the DG-in-LNP loaded with RNA and chitosan, we evaluated the pharmacologic activities with the two well-described metastatic TNBC breast cancer 4T1 and MDA-MB-231 cell lines. We found that the transfection efficiency of mRNA loaded in nanoparticle was low and not optimal. Compared to nanoparticles formulated with mRNA, the siRNA nanoparticles had much smaller size and a more stable structure: The size of siRNA nanoparticle loaded with chitosan was maintained under 150 nm, while the size of mRNA nanoparticle has exceeded 1000 nm. In MDA-MB-231

expressing luciferase reporter gene, siRNA nanoparticles with or without chitosan coating were evaluated. We discovered that the loading of PTX in nanoparticle led to 20% to 40% higher cellular luminescence signal. However, the loading of chitosan reduces the PTX-mediated increase in the luciferase's bioluminescence. Furthermore, increasing chitosan presence in nanoparticles also mitigated the toxicity associated with DG-in-LNP, thus some implication on the biocompatibility. Nanoparticles loaded with PTX showed similar cytotoxicity as free PTX form, validating the accessibility of biologic function of PTX in the DG-in-LNP. Overall, this study provides a novel approach that enables the loading of RNA molecules on stable lipid-based nanoparticle structure while enhancing the stability and targeting ability of nanoparticle.

TABLE OF CONTENTS

ACKNOWLEDGEMENTS

I would first like to express my sincere gratitude to my mentor, Professor Qingxin Mu, for his unwavering guidance and support throughout my graduate studies. His dedication to scientific rigor, coupled with his genuine care for his students, has deeply influenced my development both personally and professionally as a pharmaceutical scientist. I am truly thankful for the many opportunities he has provided and for the invaluable lessons he has shared with me. I am also incredibly grateful to Professor Rodney JY Ho, whose mentorship has been instrumental not only in my thesis work but also throughout my pharmaceutical education and research. His insights during coursework, his constructive feedback on my research, and his thoughtful guidance in shaping my thesis have significantly enriched my academic experience. I appreciate his continued support and commitment to student success at UW.

I would like to extend my heartfelt thanks to all the members of the Ho and Mu lab research teams, especially those who contributed to my project or supported me over the past two years. Collaborating with such talented and dedicated researchers has been an exceptional and formative experience—one that I will carry with me throughout my life. I am also deeply grateful to the faculty and staff of the Department of Pharmaceutics and my 2023 cohort for consistently challenging me to think critically.

Lastly, I would like to express my deepest thanks to my family and friends for their support throughout the years.

The research is supported in part by NIH and NCI grant R21 CA273739, and University of Washington (DMTSPR Consortium)

1. INTRODUCTION

1.1. Breast cancer subtypes and significance of triple-negative breast cancer (TNBC)

Breast cancer has become the most prevalent cancer in females in United States with estimated 319,759 new cases diagnosed and 42,680 deaths in 2025 (Siegel et al., 2025). Diverse subtypes of breast cancer have been discovered based on the expression level of progesterone or estrogen receptor (PR and ER) and human epidermal growth factor 2 (HER2), including hormone receptor positive, HER2 positive, and triple-negative breast cancer (TNBC) where all the above molarecular markers are absent (Vagia et al., 2020). Among the subtypes described above, hormone receptor positive composites of 70% of patients, while HER2 positive and TNBC composite of 15%-20% and 20%, respectively (Cortes et al., 2020). Chemotherapy drugs now are used as both an adjuvant and neoadjuvant therapy against TNBC patients who have received local treatment and are at higher risk for relapse (Marra et al., 2021). Regardless of the types of breast cancer, it becomes not curable once enters the metastatic stage, and the five-year survival rate of metastatic breast cancer (MBC) is only around 30% (Gavrilov et al., 2012). Compared to early stages, systemic chemotherapy is increasingly used to treat MBC, particularly when hormonal therapy proves insufficient. Existing chemotherapy drugs against breast cancer have high potency with high toxicity but have weak therapeutic effects and are easy to develop chemo-resistance in MBC patients (Hu et al., 2013). In a study published in 2012, 90% of the MBC patients were reported to show disease progression while receiving neoadjuvant chemotherapy (Chen et al., 2011). Meanwhile, the systemic use of chemotherapy was found less effective with age (Klar et al., 2019), and no survival advantage was observed in MBC patients treated with chemotherapy, resulting in a poor response of chemotherapy in MBC patients

overall (Klar et al., 2019). Comparing to other subtypes, TNBC was more challenging to treat against. Due to the lack of HER2, PR, and ER expression, TNBC is not sensitive to endocrine therapy (such as tamoxifen or aromatase inhibitors) or HER2 treatment (like trastuzumab) (Waks et al., 2019). According to the National Comprehensive Cancer Network guideline, the first-line standard regimens of TNBC were combination therapies instead of monotherapies (Gradishar et al., 2025). Meanwhile, TNBC also exhibits clinic features of high invasiveness, high metastatic potential, proneness to relapse, and poor prognosis of median survival time of 1 year comparing to approximately 5 years in other breast cancer subtypes (Waks et al., 2019).

1.2. Combination therapy against TNBC

As TNBC has low expressions of HER2, PR, and ER, endocrine therapies are less effective, and target establishment is more difficult. Despite the restrictions of systemic chemotherapy treatment against metastatic breast cancer, chemotherapy has become the major treatment against TNBC. The combination regimens based on taxanes, anthracycline, cyclophosphamide, cisplatin, and fluorouracil are recommended by the national comprehensive cancer network guidelines (Waks et al., 2019). Anthracyclines, including doxorubicin (DOX) and daunorubicin, target the 20S subunit of the proteasome and lead to the blocking of DNA replication, transcription, and relegation (Mattioli et al., 2023). Taxanes, including paclitaxel (PTX) and docetaxel, bind to β-tubulin of microtubules and stabilize it, resulting in mitosis arrest of cancer cells (Murray et al., 2012). Cisplatin binds to purine residues in DNA and prevents cell division, inducing apoptosis, while fluorouracil is an analogue of uracil and interrupt with RNA synthesis (Dasari et al., 2014; Longley et al., 2003). With varying therapeutic targets, combining different chemotherapy drugs can potentially suppress the progression of drug resistance with

reduced dosing compared to single chemotherapy treatment. For example, a phase 2 clinical trial in 2026 randomized stage II and III TNBC patients to receive PTX (175 mg/m^2, day 1) plus carboplatin (Area under the curve = 5) (Zhang et al., 2016). Pathological complete response (pCR) of 38% was reported (Zhang et al., 2016), as compared to 12% in stage I to III TNBC patients treated with taxane-based regimen only (Liedtke et al., 2008). Combined chemotherapy drug treatments might exhibit stronger therapeutic efficacy, but drug interactions showed a rate of synergy in only 0.9% of chemo-chemo combinations among pancreas, colon, and breast cancers (Jaaks et al., 2022). However, the synergy rate was increased to 3.2% and 6.1% when the combination became chemo-targeted compounds and targeted-targeted compounds, respectively (Jaaks et al., 2022).

Based on the approach of combining targeted treatments, Combinations beyond chemo-chemo, including immuno-and-chemo and gene-chemo, have demonstrated synergistic effects in various studies. (Li et al., 2017; Libson et al., 2014). For example, combining chemotherapy and immunotherapy can enhance treatment efficacy through multiple mechanisms. Chemotherapy may regulate the population of regulatory T cells and myeloid-derived suppressor cells, leading to the suppression of immune responses, which creates a more favorable microenvironment to enhance immunotherapy effectiveness. For example, in a study performed by Ramakrishnan et al. in 2010, a combination of suboptimal doses of PTX (12.5 mg/kg) and the p53 DC vaccine (100 μg plasmid DNA per mice) effectively suppressed tumor growth in the MC38 model for at least 35 days following the initiation of treatment, while PTX p53 DC vaccine solely did not show a significant therapeutic effect and PTX solely showed a resumed tumor progression after 13 days of treatment injection (Ramakrishnan et al., 2010). Additionally, by inducing cancer cell

death, chemotherapy increases tumor antigen expression and release, which enhances immune system recognition of cancer cells (Ramakrishnan et al., 2011).

Among different species of immunotherapies, immune checkpoint inhibitors (ICI) have reshaped treatment strategies across several cancers (Schoenfeld et al., 2020). In a phase 3 clinical study published in 2019 where 451 metastatic TNBC patients were treated, Metastatic TNBC patients treated with atezolizumab (840 mg per patient), a PD-L1 inhibitor, and albumin-bound nab-PTX (100 mg/m^2) had achieved median progression-free survival time (PFS) of 7.2 months while patients treated with placebo and nab-PTX showed a PFS of 5.5 months. Those numbers were 7.5 months and 5.0 months in PD-L1-positive patients, respectively (Schmid et al., 2019). The 31% and 50% increase in median PFS showed a promising therapeutic efficacy of atezolizumab combined with nab-PTX. However, in a following phase 3 clinical trial where 45% of 651 metastatic TNBC patients were PD-L1 positive, a median PFS of 6 months was observed in patients treated with atezolizumab (840 mg per patient) combined with nab-PTX (90 mg/m^2) while 5.7 months of PFS was discovered in patients treated with placebo and nab-PTX, indicating that combination of atezolizumab and nab-PTX did not improve PFS (Miles et al., 2021). Two clinical studies had 10 mg/m^2 difference in nab-PTX dosing, leading to a significant difference in therapeutic efficacy. This indicated that combination therapies of nab-PTX and atezolizumab might not be effective in all patients, and a strict dosing should be followed. Therefore, a more strictly monitored administration of ICI-chemo combination therapies with appropriate dosing was needed to enhance their therapeutic efficacy.

Despite its use in combination therapies against TNBC, immunotherapy is facing drug resistance challenges. For example, after repeated dose, ICIs were reported to show acquired resistance, which showed deficiency in antigen presentation and interferon-γ (IFN-γ) signaling

(Schoenfeld et al., 2020). For example, in a study published in 2016, a patient treated with pembrolizumab, a PD-1 inhibitor, was discovered acquiring a beta-2-microglobulin mutation, leading to major histocompatibility complex 1 destabilization, which enabled the escape of tumor from immune detection (Zaretsky et al., 2016; Restifo et al., 1996). In the same study, 2 patients had melanoma progression 1 and 2 years after treated with pembrolizumab. The acquired mutation *JAK1* or *JAK2* after treatment was discovered in those patients, inducing a loss of tumor cell sensitivity to IFN-γ (Zaretsky et al., 2016). Moreover, the loss of PTEN, a commonly mutated tumor suppressor gene, has been associated with a 50% smaller reduction in tumor size compared to patients with stage IIIB/C melanoma that retained PTEN expression (Peng et al., 2016). Besides the drug resistance induced by immunotherapy, the use of combination therapy requires strict administration to avoid the accumulation of toxicity (Ramakrishnan et al., 2011). Therefore, alternative therapies might be explored to overcome the challenges that existed in immunotherapies.

1.3. Therapeutic nucleic acids in MBC therapy and challenges in delivery

Increasing analyses in cancer cell chromosomes has suggested that specific types of cancers are linked to distinct and recurring genetic abnormalities (Stratton et al., 2009). Delivering nucleic acid molecules into mutated cells has gained increasing attention, as it addresses the problem at its source and has the potential to overcome drug resistance. (Markman et al., 2013). Messenger RNA (mRNA), a single stranded nucleic acid molarecule derived from DNA transcription, carries the genetic code and promotes its translation into amino acids. mRNA provides various directions in treating against cancer, including expressing tumor suppressor proteins to restore wildtype genes, encoding cytokines to enhance the immune response against

cancer, and enhancing chimeric antigen receptor expression in T cells to achieve greater tumor cell detection (Liu et al., 2023). Small interfering RNA (siRNA), a double-stranded nucleic acid molarecule, can silent the target gene. siRNA has been explored to regulate mutated genes in different cancers (Hu et al., 2020). Moreover, siRNA can be used to overcome drug resistance. For example, in a study performed in 2013, siRNA of myeloid cell leukemia-1 (Mcl-1), which led to higher resistance of DOX, down-regulated its expression to around 20%, and might resulted in enhanced DOX sensitivity (Aliabadi et al., 2013).

The *in vitro* transcribed mRNA provides significant versatility as a form of cancer therapy by allowing the generation of target proteins without altering the genome, thus is used as a type of therapeutics (Liu et al., 2023). Novel approaches that focus on more unique variations between cancer cells and healthy cells have been discovered, such as cells with PTEN presence or absence (Raza et al., 2021). PTEN mRNA expression in TNBC cell line, 4T1, was 4-fold lower compared to that in BT-474, a PTEN-competent cell line (Kim et al., 2024). In this study in 2024, 1.5 μg/mL PTEN mRNA was delivered into 4T1-Luc (Luciferase edited) cells and showed a 30% cell knock out. Meanwhile, a 40% and 50% 4T1-Luc cell knockout were observed when the concentration of PTEN mRNA increased to 1.5 μg/mL and 3 μg/mL, indicating a dose-dependent cell knockout by PTEN mRNA restoration (Kim et al., 2024).

Comparing to plasmid DNA, mRNA exhibits greater *in vitro* transcription. Lower toxicity and higher translatability are observed in mRNA since entering the nucleus is not required to internalize mRNA into the cells; mRNA also has higher transfection efficiency than DNA, leading to a higher protein expression level; and mRNA transfection avoids insertional mutagenesis since its transfection is not integrated into the genome sequence (Zhang et al., 2019). However, the considerable size of mRNA (300-1500 kDa) and its negatively charged

structure prevent the permeation of naked mRNA across the cell membrane (Zhang et al., 2019). Besides, mRNA is also prone to degradation, inducing the incapability to be efficiently released into cytoplasm (Gavrilov et al., 2012).

Besides mRNA, siRNA is also used as effective therapeutics (El Moukhtari et al., 2023). In a study in 2022, siRNA (100 nM) targeting IKBKE were delivered in lipid nanoparticle and induced 60% decrease in gene expression in PANC-1 cells and 80% decrease in PANC02 cells (Patel et al., 2022). Comparing to mRNA, siRNA has a smaller molarecular size and is double stranded, enhancing the stability and making the delivery easier (van den Bent et al., 2002; Alkekhia et al., 2020).

1.4. The significance of drug-gene co-delivery and its delivery approaches

To overcome the biological barriers of nucleic acid molarecule delivery, different strategies have been explored to develop its delivery into targeted cells. Chemical modifications of RNA, including base and sugar-phosphate backbone modifications, greatly enhanced the stability of nude RNA molecules (Gupta et al., 2021). However, reduced target specificity and acquired translation disruption prevented siRNA from being an excellent therapeutic nucleic acid (Gupta et al., 2021; Karikó et al., 2005). Various delivery vehicles were also developed to deliver RNA molecules, such as virus vectors, polymers, and lipid-based nanoparticles. Virus vectors exhibited effective delivery of nucleic acids into targeted cells but were also capable to interact with host genome and resulted in enhanced genotoxicity (Young et al., 2006; Kotterman et al., 2014). Polymeric nanoparticles have been explored and there were various designs that efficiently delivered nucleic acid molecules. For example, a poly(amidoamine) dendrimer was

reported to efficiently deliver plasmid DNA into CV-1, HeLa, and HepG2 cells (Haensler et al., 1993). Moreover, poly(lactic-co-glycolic acid) was also proofed to encapsulate and deliver siRNA molecules (Singha et al., 2011). Lipid-based nanoparticles (LNPs) are widely studied, with the most common liposomal structures incorporating a combination of lipids to optimize delivery. In this system, phospholipids facilitate endosomal escape, while ionizable lipids and helper lipids work together to protect nucleic acid cargo from degradation and ensure structural stability of the nanoparticle (Gupta et al., 2021).

While a variety of nanocarriers of nucleic acid molecules have been developed, the presence of a carrier also enables the co-delivery of nucleic acids with chemotherapy drugs to reach synergistic effects against cancer. In a study performed by Zhang et al. published in 2019, nanoparticles loaded with p53 mRNA and PTX exhibited 4-fold decrease in tumor size with 70% higher survival rate in mice comparing to PTX or mRNA loaded nanoparticle alone (Zhang et al., 2019). In another study done by Li et al., microRNA21, which upregulates tumor suppressor genes PDCD4 and PTEN, was co-delivered with a chemotherapy drug called gemcitabine. The result showed a 6-fold decrease in both tumor volume and weight in mice comparing to drug or microRNA21 loaded nanoparticle only (Li et al., 2017). In a study performed by Jiang et al. in 2023, DDIT4-AS1, which is highly expressed in TNBC cells due to H3K27 acetylation, was targeted. A core-shell nano system was used to co-deliver siRNA and PTX and showed a 40% increase in cell death as anti-DDIT4-AS1 siRNA enhanced the sensitivity to PTX of cells (Jiang et al., 2023).

1.5. GT-in-DcNP for enhanced drug delivery and therapeutic efficacy

The nanoparticle design in this thesis project was built on a drug combination lipid-based nanoparticle DcNP platform composed of gemcitabine (GEM or G) and PTX (or T) combination in DcNP referred to as GT-in-DcNP. GT-in-DcNP has been shown to provide long-acting and synchronized exposure to breast tumor in the lung and in the fat-pad leading to optimal tumor suppression and in some cases regression (Mu et al., 2020; Perazzolo et al., 2020; Yu et al., 2020; Yu et al., 2024). The original lipid components of DcNP include 1,2-Distearoyl-sn-glycero-3-phosphocholine (DSPC) and 1,2-distearoyl-sn-glycero-3- phosphoethanolamine-N-[amino (polyethylene glycol)-$_{200}$0] (ammonium salt) (DSPE-mPEG$_{2000}$). GT-DcNP enabled the co-delivery of PTX and Gemcitabine (GEM) against TNBC and showed efficacy in 4T1-Luc cells and BALB/c mice (Mu et al., 2020).

Liposome (>200 nm) was experiencing the premature clearance and might resulted in poor targeting to cancer cells. Meanwhile, some small polymeric nanoparticles or micelles (<10 nm) would undergo renal filtration and resulted in an early elimination and short half-life. GT-DcNP, with a consistent size of around 50 nm, had different structure compared to other lipid-based nanoparticles. Despite its desirable size, GT-in-DcNP was also able to co-load water soluble GEM and water insoluble PTX and resulted in successful delivery and release into TNBC cells. GT-in-DcNP also had straight forward manufacturing process, where drug purification was not needed (Mu et al., 2020; Perazzolo et al., 2020; Yu et al., 2020; Yu et al., 2024).

GT-in-DcNP showed a significant pharmacokinetics profile (Yu et al., 2020). In a non-compartmental analysis, an 8.6-fold increase of half-life from 1.6 hour in Cremophor EL (crEL) as a control to 13.7 hours in DcNP was observed in GEM with 61-fold increase in total exposure

(AUC) compared to crEL, indicating that GEM was highly associated *in vivo*. Meanwhile, AUC of 3.8-fold increase with no significant change in half-life was discovered in PTX delivered with compared to crEL. This result suggested that DcNP showed great stability *in vivo* and prolonged the circulation time of GEM and PTX, achieving a lower systemic toxicity and enhanced drug exposure to tumor (Yu et al., 2020).

Besides desirable pharmacokinetics properties, GT-in-DcNP also showed great efficacy and safety. In 4T1 mice model, a single dose of GEM (20 mg/kg) and PTX (2 mg/kg) in DcNP achieved approximately complete elimination of tumor colonization in lung metastasis, while the dose of GEM (100 mg/kg) and PTX (10 mg/kg) in crEL was not able to show similar efficacy (Mu et al., 2020). Furthermore, GT-in-DcNP also had a therapeutic index of 15.8, indicating that GT-in-DcNP had good safety profile (Mu et al., 2020; Tamargo et al., 2015).

However, the formulation of GT-in-DcNP was not designed to co-load nucleic acid molecules with chemotherapy drugs. To further enhance the pharmacokinetic properties and therapeutic efficacy against TNBC, the structure of GT-in-DcNP needed further exploration to enable the loading of nucleic acid molecules with its desired drug release and circulation time.

1.6. Layer-by-layer approach of drug-gene nanoparticle preparation

Layer-by-layer (LbL) is an approach that utilizes electrostatic interactions between oppositely charged polymeric compounds, such as negatively charged DNA or RNA polymer binding to positively charged polymers or lipid-nanoparticles to promote the self-assembly of nanoparticle intended to enhance stabilization of genetic drugs such as siRNA and mRNA and promote intra-cellular entry for pharmacological effects (Alkekhia et al., 2020). Besides nucleic

acid polymers like RNA and DNA, LbL structure also enabled the loading of versatile therapeutic agents, including small molarecule drugs and enzymes or proteins (Alkekhia et al., 2020). LbL structure was also reported to enhance the stability and biocompatibility of nanoparticle (Shaabani et al., 2021). In the study performed by Shabbani et al., The colloidal stability of gold nanoparticle loaded with chitosan and siRNA layers (LbL-CS-AuNP) was compared with that of siRNA loaded nanoparticle prepared with chitosan alone (CSNP). LbL-CS-AuNP maintained a stable size of around 90 nm for 168 hours, while the size of CSNP increased to 700 nm at the same time. LbL-CS-AuNP also showed a complete siRNA release in HEPEs buffer at 37 ◦C while the maximum release of siRNA in CSNP was around 20%, and all the results suggested that a greater stability was achieved in AuNP with LbL loading of siRNA and chitosan (Shaabani et al., 2021).

In addition to enhanced stability and biocompatibility, LbL nanoparticle that co-delivered chemotherapy drugs and therapeutic nucleic acid molecules showed enhanced efficacy against tumors along with desirable pharmacokinetics profile. In a study performed by Deng et al in 2013, DOX loaded liposome nanoparticles (1 mg/kg of DOX) were prepared as the core. On the outside of this negatively charged nanoparticle core, layers of polycation and siRNA (1 mg/kg) was loaded alternatively using electrostatic interactions between positive and negative charges. Multidrug resistance protein 1-siRNA (MRP1), which silenced MRP1 expression and enhanced the efficacy of DOX, was incorporated in this LbL nanoparticle. On the outside of nanoparticle, cationic poly-L-arginine (PLA) was further loaded to achieve higher silencing efficiency and lower cytotoxicity. This LbL structured nanoparticle achieved a 50% tumor size reduction at 20 days of treatment, while MRP1 siRNA solely and saline showed tumor size growth to 450% and

650%, respectively. Besides, the half-life of this LbL liposome nanoparticle has reached the half-life of 28 hours and a sustained release of siRNA over 72 hours (Deng et al., 2013).

Different charged polymers can be used as the outer layer protection of LbL nanoparticles, such as polyethy-leneimine, PLA, hyaluronic acid (HA), and chitosan (Alkekhia et al., 2020). chitosan, a cationic natural derived polysaccharide, is marked due to its great biocompatibility and low toxicity (Jafernik et al., 2023). With its high degradability and biocompatibility, chitosan is one of the most used polymers to coat nanocarriers and achieve a more sustained release of charged polymers in each layer with a greater cellular uptake (Shaabani et al., 2021). Another example of polymer used in LbL composition is HA, a negatively charged polysaccharide ligand. HA is capable to stabilize nanoparticle charge and has high biocompatibility and is therefore frequently incorporated into LbL nanoparticles to enhance structural stability and achieve higher cellular uptake (Alkekhia et al., 2020). Besides, HA also has high affinity to CD44 receptors, which are highly expressed in different tumor cells (Puluhulawa et al., 2022). This makes HA a desired targeting ligand, resulting in enhanced targeting ability of nanoparticle (Puluhulawa et al., 2022). As the LbL method offers exceptional structural flexibility, it becomes a highly adaptable platform for developing multifunctional nanoparticles tailored to specific therapeutic needs.

Based on this structure, cationic lipid DOTAP is selected to convert the original structure from negatively to positively charged, enabling the loading of nucleic acids on the nanoparticle surface by electrostatic interactions. In addition, cholesterol was utilized in formulation design to enhance nanoparticle stability. chitosan was used as the out-layer protection to prevent degradation of nucleic acid molecules. HA was selected to modulate the negative charges in

nanoparticle to enable the loading of cationic chitosan on the surface of nucleic acid molarecule loaded nanoparticle.

1.7. Study objective and design

The objective of this study is to modify lipid nanoparticle structure to co-load PTX and RNA molecules to achieve a greater knockout of TNBC cells, given the difficulty to effectively treat against TNBC due to low expression of hormone receptors and HER2. Cationic lipid DOTAP was incorporated to enable the RNA molarecule loading, and chitosan was coated on the outside of nanoparticle to stabilize it and protect RNA molecules from degradation. This study developed a lipid-nanoparticle approach based on previously developed GT-DCNP, enabling the loading of RNA molecules on this lipid nanoparticle structure by LbL approach to enhance its therapeutic efficacy in TNBC cells knockout. The study includes two Aims: 1) To prepare and characterize drug-free and drug-loaded nanoparticles with varying compositions for their physicochemical properties and RNA loading; 2) To optimized RNA-drug combination nanoparticle candidates to inhibit TNBC cell growth for transfection efficiency of mRNA and siRNA in TNBC cell lines. The overall design and compartments of this drug-gene combination in lipid nanoparticle (DG-in-LNP) was presented in **Scheme 1**.

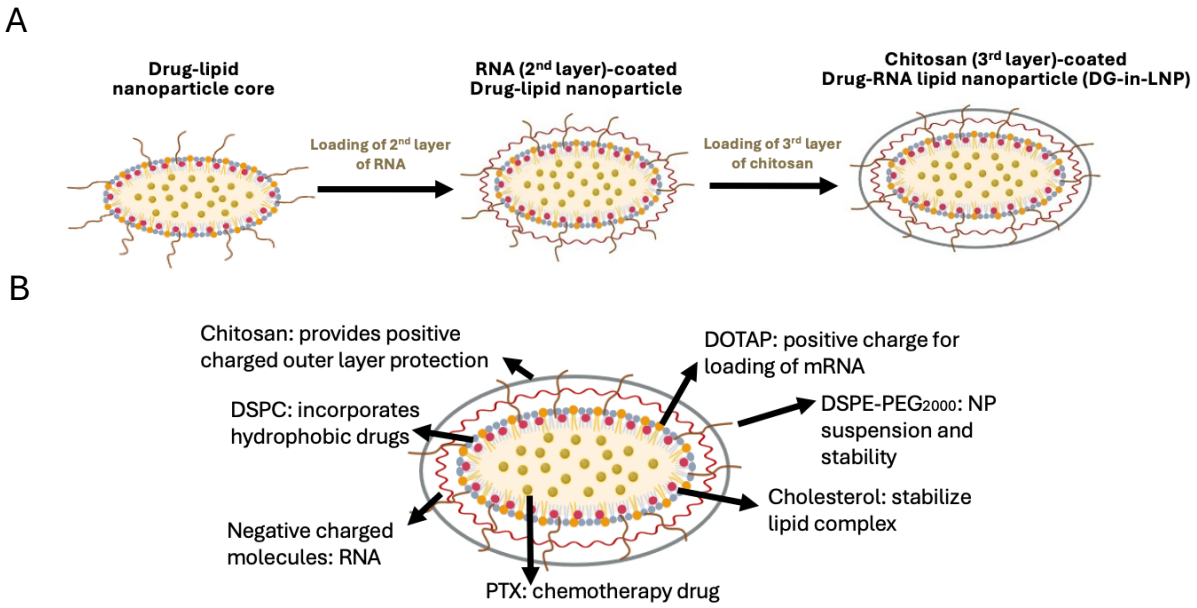

Scheme 1. *Design of a DG-in-LNP platform approach through the LbL approach.* ***(A)*** *Electrostatic adsorption of RNA molarecule and chitosan was used to functionalize a LbL lipid-based particle indicating layers of alternating charge composition.* ***(B)*** *Components of DG-in-LNP with function of each.*

2. MATERIALS AND METHODS

2.1. Materials

1,2-distearoyl-sn-glycero-3-phosphocholine (DSPC) and 1,2-distearoyl-sn-glycero-3-phosphoethanolamine-N- [amino (polyethylene glycol)-2000] (ammonium salt) (DSPE-PEG_{2000}) (GMP grade) were purchased from LIPOID (Ludwigshafen, Germany); paclitaxel (>99.5%; CAS 33069-62-4) were purchased from LC Laboratories (Woburn, Massachusetts);

1,2-dioleoyl-3-trimethylammonium propane (DOTAP) chloride were purchased from MedChemExpress (Monmouth Junction, NJ); Cholesterol were puechased from Sigma-Aldrich (Burlington, MA); DOTAP in chloroform were purchased from Avanti Polar Lipids (Birmingham, AL); HA sodium salt from Streptococcus equi, 8-15 KDa were purchased from Matexcel (Shirley, NY); chitosan (kDa 7-15) was purchased from Acmey Industrial (Shanghai, China); Lipofectamine™ RNAiMAX Transfection Reagent and Lipofectamine™ 2000 Transfection Reagent were purchased from Thermo Fisher scientific (Waltham, MA); Alamar blue reagent were purchased from Invitrogen (Waltham, Massachusetts); Roswell Park Memorial Institute (RPMI) 1640, Dulbecco's Modified Eagle Medium (DMEM), Optimized Minimum Essential Medium (Opti-MEM), HEPEs buffer, and TrypLE Express were purchased from Gibco (Waltham, MA); mCherry mRNA were purchased from PackGene Biotech (Houston, TX); firefly luciferase siRNA with sequence of (Anti-Luciferase: Length: 21 nt. Sense: 5'-CUUACGCUGAGUACUUCGAdTdT-3' Antisense: 5'-UCGAAGUACUCAGCGUAAGdTdT-3') were purchased from Horizon Dharmacon (Lafayette, CO); D-Luciferin was purchased from Perkin Elmer (Waltham, MA, USA). All other reagents used were of analytical grade or higher.

2.2. Evaluate lipid compositions of nanoparticle to optimize nucleic acids loading

2.2.1. Device and materials used to evaluate the process and compositions to optimize DG-in-LNP core formulation and loading of RNA molecules.

The average size and zeta potential of DG-in-LNP core was determined by a Malvern DLS Zetasizer Nano ZS (Malvern panalytical, Westborough, MA). HEPES buffer was diluted to 20 mM in ultrapure water and the pH was around 7.4. To measure the average size of DG-in-

LNP core, 780 μL of HEPES buffer was added into the cuvette, followed by uniformly adding and mixing 20 μL of precursor nanoparticle into the HEPEs buffer, and Z-average (nm) was recorded. After size measurement, 770 μL of NP solution was transferred from the cuvette to a folded capillary zeta cell cuvette to measure the zeta potential of the mixture.

To prepare the mRNA loading on DG-in-LNP core measurement, HA (20 mg/mL) of the amount according to different ratios was added into 780 μL of HEPEs buffer in a cuvette, and 10 μL of precursor nanoparticle (44.63 mg/mL) was mixed well with 2 μL of mRNA (1.1 mg/mL) in a 1.5 mL centrifuge tube, following the PTX:mRNA weight/weight (w/w) ratio of 5:1. Then the mRNA loaded DG-in-LNP mixture was transferred into HEPEs buffer with HA in the cuvette to form mRNA and HA loaded DG-in-LNP with NP:HA w/w ratio of (No HA, 40:1, 10:1, 7.5:1, 5:1, 4:1, 3.5:1, 3:1, 2.5:1) he Z-average of mRNA and HA loaded DG-in-LNP was measured. After size measurement, 770 μL of mRNA and HA loaded DG-in-LNP mixture was transferred from the cuvette to a zeta potential cuvette to measure the zeta potential of the mixture.

To prepare the siRNA loading on DG-in-LNP core measurement, amount of siRNA (1 mg/mL) corresponding to the desired PTX:siRNA w/w ratios (5:1, 2:1, 1:1) was added individually into different cuvettes. Then 20 μL of precursor nanoparticle (44.63 mg/mL) was pipetted into the siRNA solution and mixed well to form siRNA loaded DG-in-LNP mixture. 780 μL of HEPEs buffer (20 mM) was then added into the mixture, and the Z-average was measured. After size measurement, 770 μL of siRNA loaded DG-in-LNP mixture was transferred from the cuvette to a zeta potential cuvette to measure the zeta potential of the mixture.

To prepare the siRNA and chitosan loaded DG-in-LNP measurement, 21.4 μL of siRNA (1 mg/mL) was added into the cuvette. Then 20 μL of precursor nanoparticle (44.63 mg/mL) was

pipetted into the siRNA solution and mixed well to form siRNA loaded DG-in-LNP mixture. The following step was adding corresponding amount of chitosan (1 mg/mL) into the cuvette and mixing with siRNA loaded DG-in-LNP to form siRNA and chitosan loaded DG-in-LNP at different PTX:siRNA:CHI w/w ratios (1:1:1, 1:1:2, 1:1:5, 1:1:10), and the Z-average was measured. After size measurement, 770 µL of DG-in-LNP mixture was transferred from the cuvette to a zeta cell and the zeta potential was determined.

2.2.2. Preparation of lipid nanoparticle with varying DOTAP molarar ratio to test its effect on nanoparticle size and charge

The base composition in molar ratio of DSPE- PEG_{2000}(10%), and PTX (1:40 molar ratio to lipid) was fixed, while the composition of DOTAP and DSPC made up the rest 90% of lipids. DG-in-LNP core with DSPC of (90, 80, 60, 40, 20 molar %) and DOTAP of (0, 10, 30, 50, 70 molar %, Avanti Polar Lipids) were prepared, and the formulation was presented in **Table 1**.

DG-in-LNP core was prepared by the same thin-film methods as described in (Shaabani et al., 2021; Cocco, 2022). Briefly, all the lipid components were dissolved in ethanol (20 mg/mL) in a round bottom flask. Then the ethanol was removed by rotatory evaporator. The flask was rotated at 250 rpm in 60 °C water and at different vacuum pressure level (250, 400, 600 mmHg) for 5 minutes respectively. After the solvent has been removed, lipid component formed a thin-film and was further desiccated to remove remained solvent by vacuum overnight. The thin-film was then rehydrated in saline at 70 °C in oil bath for 3 hours. Immediately after rehydration, the mixture was sonicated by a Branson 2800 bath sonicator at 42 °C and the highest power for 5 minutes and returned to oil bath for another 5 minutes to reduce its size. This

procedure was repeated for 2 times (3 cycles in total) and no return to oil bath was needed in the last cycle. Then the nanoparticle precursor (44.63 mg/mL) was stored at 4 °C.

Table 1. The composition of DG-in-LNP core formulation #1-5 with increasing fractions of DOTAP to evaluate the surface charge and enable the loading of negatively charged RNA molecules.

Nanoparticle #	DSPC % mol	DOTAP % mol	DSPE-PEG_{2000} % mol	PTX:lipid mol ratio
1	90	0	10	1:40
2	80	10	10	1:40
3	60	30	10	1:40
4	40	50	10	1:40
5	20	70	10	1:40

2.2.3. Preparation of lipid nanoparticles in different rehydration media and test the impact of saline as rehydration solvent in nanoparticle size and charge

The solvent removal and size reduction procedures were carried out as described in 2.2.2. section. Nanoparticle with lipid component of DSPE-PEG_{2000} (10%), PTX (1:40 molar ratio to lipid), DSPC (40%), and DOTAP (50%, Avanti Polar Lipids) was selected and rehydrated in both saline and ultrapure water with same procedure.

2.2.4. Preparation of lipid nanoparticle with or without PTX loading and test its impact in nanoparticle size and charge

The solvent removal and size reduction procedures were carried out as described in 2.2.2. section. Nanoparticles formulation of DSCP (70%, 60%, 50%, 40%) and DOTAP (20%, 30%, 40%, 50%, Avanti Polar Lipids) were rehydrated in ultrapure water and their size and zeta potential were measured. For every formulation, nanoparticle with PTX and without PTX loading were all prepared and tested. The compartment of each formulation was presented in **Table 2**.

Table 2. The composition of DG-in-LNP core #6-9 with or without chemotherapy drug PTX to test the effect of PTX loading in DG-in-LNP core on nanoparticle size and surface charge along with uniformity by PDI.

Nanoparticle #	PTX	DSPC % mol	DOTAP % mol	DEPE- PEG_{2000}% mol	PTX % mol
6	Yes	70	20	10	1:40
6	No	70	20	10	0:40
7	Yes	60	30	10	1:40
7	No	30	30	10	0:40
8	Yes	50	40	10	1:40
8	No	40	40	10	0:40
9	Yes	40	50	10	1:40
9	No	40	50	10	0:40

2.2.5. Preparation of lipid nanoparticle with cholesterol and test its impact in nanoparticle size and charge

The solvent removal and size reduction procedures were carried out as described in 2.2.2. section. The base composition in molarar ratio of DSPE-PEG_{2000} (10%), and PTX (1:40 molar ratio to lipid) was fixed, while 20 molar % of DSPC was substituted by 20 molar % of cholesterol. Cholesterol containing nanoparticles with lipid formulation of DSPC (50%, 45%) and DOTAP (20%, 25%, MedChemExpress) were prepared and tested. Nanoparticle with DSPC (65%), DOTAP (25%, MedChemExpress), DSPE- PEG_{2000} (10%), and PTX (1:40 to lipid) was selected as a control. The compartment of formulations tested were presented in **Table 3**.

Table 3. The composition of DG-in-LNP core #14 and 15 with cholesterol loaded and to evaluate potential size reduction and increase in surface charge measurement by zeta potential.

Nanoparticle #	DSPC % mol	DOTAP % mol	DEPE- PEG_{2000} %	Cholesterol % mol	PTX % mol
14	50	20	10	20	1:40
15	45	25	10	20	1:40

2.3. Process of siRNA and mRNA loading on nanoparticle

mRNA was diluted in ultrapure water (1.1 mg/mL) and transferred to a 1.5 mL crimp vial with a stir bar. The nanoparticle precursor (44.63 mg/mL of lipid compartments) was slowly pipetted into mRNA solutions while stirring at 300 rpm at room temperature to form a homogenous mRNA loaded DG-in-LNP mixture. HA (1 mg/mL) was pipetted into the same vial according to PTX:mRNA w/w ratio of 5:1 and reached different NP:HA w/w ratios (40:1, 10:1,

7.5:1, 5:1, 4:1, 3.5:1, 3:1, 2.5:1). These ratios were selected for mRNA loading on nanoparticle core.

The mRNA and HA loaded DG-in-LNP mixture was slowly pipetted into chitosan solution (1 mg/mL) while stirring at 300 rpm to form the mRNA, HA, and chitosan loaded DG-in-LNP mixture. The mRNA, HA, and chitosan loaded DG-in-LNP mixture was added at a small amount per time for multiple times.

To load siRNA on the surface of nanoparticle precursor, siRNA was first diluted in ultrapure water (1 mg/mL) and transferred to a 1.5 mL centrifuge tube. The nanoparticle precursor (44.63 mg/mL) was quickly added into siRNA solution and thoroughly mixed by repeatedly pipetting to form a homogenous suspension. PTX:siRNA w/w ratio of (5:1, 2:1, 1:1) were selected to evaluate formulation stability and surface charge.

siRNA loaded DG-in-LNP mixture was pipetted into chitosan solution (1 mg/mL) and thoroughly mixed to form the homogenous siRNA and chitosan loaded DG-in-LNP suspension. PTX:siRNA:CHI w/w ratio of (1:1:1, 1:1:2, 1:1:5, 1:1:10) were selected to evaluate formulation stability and surface charge.

2.4. Cell study

2.4.1. Cell culture

All cell lines were obtained from Houston Methodist Academic Institute and Fred Hutchinson Cancer Research Center. All cells were cultured at 37 °C and 5% CO_2 (95% humidity). Human triple-negative breast cancer MDA-MB-231 cells and MDA-MB-231-luc

(luciferase edited MDA-MB-231 cells) were cultured in a DMEM medium with 10% fetal bovine serum and 0.5 % anti-anti. Cells were passaged by treatment with TrypLE Express.

2.4.2. In vitro mRNA and siRNA transfection

To evaluate transfection efficiency of mRNA by nanoparticles, mCherry mRNA was selected as the model molarecule. 4T1 cells were seeded at a density of 4,000 cells/cm^2 in clear-bottomed Corning 48-well cell culture plates with 250 μL of the cell culture medium the day before adding different treatments. The cells were incubated with treatments for 24 hr after overnight attachment and were imaged with a Nikon TE300 inverted fluorescent microscope.

Treatments included negative and positive control and mRNA loaded nanoparticle. Lipofectamine 2000-mRNA complexes were added to cell culture according to manufacturer's protocol as a positive control. No treatment (cells only) was selected as a negative control. Treatment groups were mRNA only, mRNA and HA loaded DG-in-LNP, mRNA, HA, and chitosan loaded DG-in-LNP, and nanoparticle core only. The amount of mCherry mRNA (1.1 mg/mL) was fixed at 1 μg in each well, including positive control group and treatment group.

To evaluate transfection efficiency of siRNA loaded DG-in-LNP, and siRNA and chitosan loaded DG-in-LNP, Luciferase siRNA (siLuc) was selected as the model siRNA and MDA-MB-231-Luc cell line was selected. MDA-MB-231-Luc cells were seeded at a density of 45,000 cells/cm^2 in 96-well plates with 100 μL of the cell culture medium the day before adding treatment groups. Both cell lines were incubated with treatment groups for 24 hr after overnight attachment. To enable the exhibition of luciferase luminescence, cell culture medium was aspirated off and replaced with 110 μL of the mixture of fresh cell culture medium with D-luciferin at the final concentration of 3 mg/mL. The plate of MDA-MB-231-Luc cells was

analyzed using a (model) plate reader at wavelength of 578 nm with bandwidth emission of 15 nm. Luminescence was recorded after a 5-minute incubation using a microplate luminometer.

Treatments included negative and positive control and mRNA loaded nanoparticle. Lipofectamine RNAiMax-siRNA complexes were added to wells needed according to manufacturer's protocol as a positive control, while free PTX (1.71, 0.68, 0.34 µg/mL) were also used as a positive control. No treatment (cells only) and free chitosan (0.68, 1.71, 3.42 µg/mL) were selected as a negative control. Treatment groups were siRNA loaded, siRNA and chitosan loaded DG-in-LNP while PTX loaded and PTX free nanoparticle of each ratio were all included. The amount of siLuc (1 mg/mL) was fixed at 0.53 µg in each well, including positive control group and treatment group, and all treatments were triplicated. The procedure of *in vitro* transfection and evaluation methods were presented in **Scheme 2**.

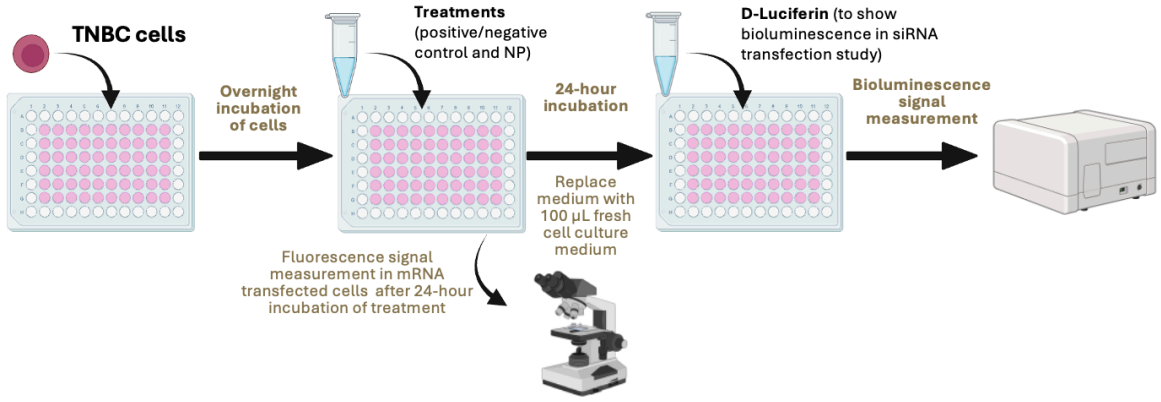

Scheme 2. *Workflow of evaluating in vitro transfection of RNA molecules loaded on nanoparticles.*

2.4.3. Cytotoxicity

Cell viability was evaluated using Alamar blue assay (Rampersad, 2012). Cells at same amount and density per well were prepared in a clear-bottomed Corning 96-well cell culture

plate and were administered with same treatments in 2.4.2. and incubated for 24 hours. Similarly, all treatments were triplicated. To do this, medium was removed and replaced with the mixture of 12 µL Alamar blue reagent and 108 µL cell culture medium per well and was incubated at 37 °C and 5% CO_2 for 4-5 hours until an obvious color change was observed. After incubation, 100 µL of Alamar blue reagent-cell culture medium mixture was transferred to a black recovery plate. The results were obtained from Spectramax i3 plate reader from Molarecular Devices at 578 nm with a bandwidth emission of 15 nm for 500 ms.

2.5. Statistical analysis

Nucleic acid transfection efficiency data were presented as the arithmetic mean ± standard error of the mean (SEM). All treatments in cellular studies were triplicated. Statistical analysis was performed using GraphPad Prism 10.4.0 (GraphPad Software Inc., San Diego, CA). One-way ANOVA was used to determine statistical significance for multiple treatment groups across studies. A P-value of ≤ 0.05 was considered statistically significant.

3. RESULTS AND DISCUSSION

3.1. Nanoparticle carrying positive charge to enable loading and stabilization of nucleic acid molecules

3.1.1. Effects of substituting structural lipid DSPC with cationic lipid DOTAP in nanoparticle size and charge

The formulation of DG-in-LNP core was characterized by nanoparticle average size and zeta-potential. DG-in-LNP core # 1-5 were rehydrated in saline. The composition of each formulation is listed in table 1 as molarar percent, and the results are presented in **Table 4** and in **Figure 1**.

Table 4. The Effect of increasing cationic DOTAP in nanoparticle lipid composition on surface potential-positively charge measured by zeta potential along with size and uniformity by PDI in nanoparticle #1-5.

Nanoparticle # - (% of DOTAP)	Z-average (nm)	PDI	Zeta potential (mV)
1 (0)	112.7	0.16	-14.0
2 (10)	95.0	0.16	-12.3
3 (30)	110.5	0.23	-8.7
4 (50)	139.2	0.25	+5.6
5 (70)	138.2	0.29	+18.6

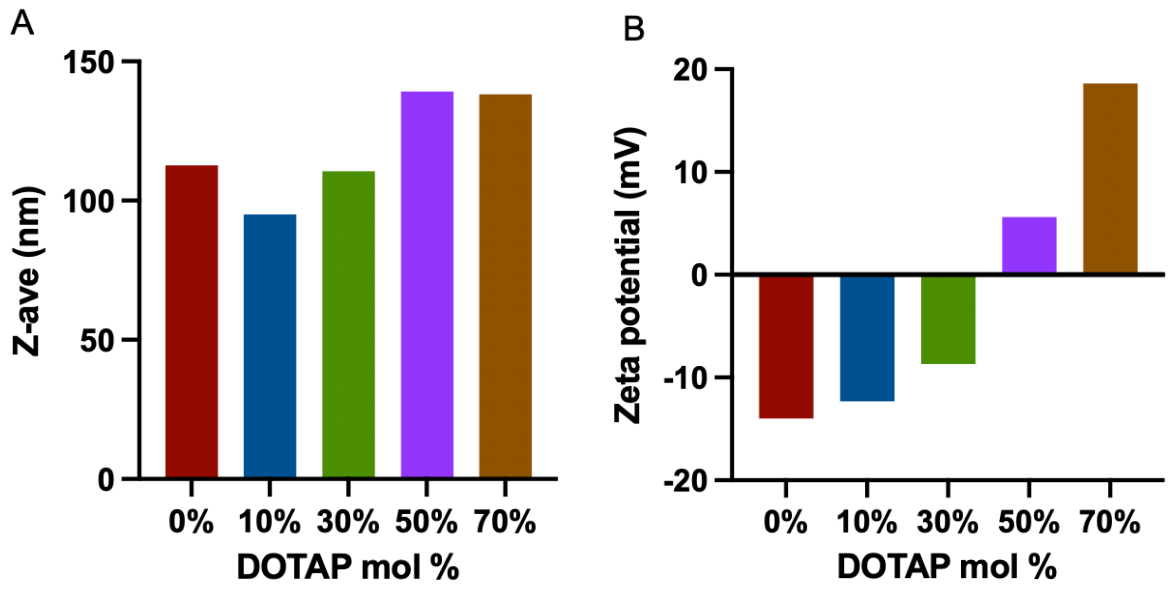

Figure 1. *The effect of increasing cationic DOTAP in nanoparticle lipid composition on surface potential-positively charge measured by zeta potential along with size and uniformity by PDI.* ***(A)*** *The Z-average of DG-in-LNP core formulation #1-5.* ***(B)*** *The zeta potential of DG-in-LNP core formulation #1-5.*

With the increasing molar ratio of DOTAP in lipid components, an overall trend of increased average size was observed. The structure of DOTAP induced concerns regarding the overall stability of DG-in-LNP core. Each carbon chain of DOTAP contained a double bond between carbon 9 and carbon 10, inducing a more flexible structure and lower phase transition temperature of DG-in-LNP core, and therefore decreased the stability of its structure (Meisel et al., 2016). As the presence of double bonds in carbon chains created more intramolarecular spaces between each fatty acid molecules, increasing DOTAP molar ratio, which represented increasing double bond contents in lipid nanoparticle core, led to an increase in the nanoparticle average size. Meanwhile, an obvious trend of increasing zeta potential was observed with the increasing amount of DOTAP in lipid compositions. Each DOTAP molarecule contain a quaternary ammonium group, introducing a positive charge to the nanoparticle lipid structure,

and this expected observation confirmed the successful mixing of DOTAP into lipid structure of nanoparticle (Meisel et al., 2016). An overturn of zeta potential from negative to positive was observed from nanoparticle #3 and 4, which contained a 20% difference in DOTAP molar percent. This observation indicated that adding DOTAP into formulation was able to overturn the originally negatively charged nanoparticle structure to positively charged. In this way, the positively charged DG-in-LNP core structure enabled the loading of negatively charged nucleic acids using layer-by-layer method.

3.1.2. Impact of saline solution on average size and charge in nanoparticle rehydration

Saline solution, which contained sodium and chloride ions to avoid ion concentration disturbance while expanding intravascular volume in human body, was used to rehydrate nanoparticles (Patel et al., 2025). As described in the method and material section above, zeta potential of nanoparticle was measured by Malvern DLS Zetasizer Nano ZS. According to its user's manual, zeta potential was measured by the velocity of charged particles move in a liquid when an electrical field is applied (Malvern, 2013). While the zeta potential measured the surface charge of nanoparticles, the ions in saline solution might interrupt with the measurement, leading to an inaccurate result. Therefore, it was necessary to investigate the impact of rehydrating nanoparticles using saline solution for nanoparticle rehydration step.

The impact of using saline or ultrapure water to rehydrate DG-in-LNP core was studied using the same method described above. Nanoparticle #4 was rehydrated in both saline and ultrapure water. The average size of nanoparticle rehydrated in saline was 139.2 nm and was 142.8 nm in ultrapure water. While the average size was not impacted by using different rehydration solvent, the zeta potential of nanoparticle rehydrated in saline was +5.6 mV compared to +16.1 mV in ultrapure water. As DG-in-LNP core was rehydrated in saline, the Na^+ and Cl^- ions in saline shielded the surface charge of DG-in-LNP core, leading to a lower zeta potential measurement. The result was shown in **Figure 2**.

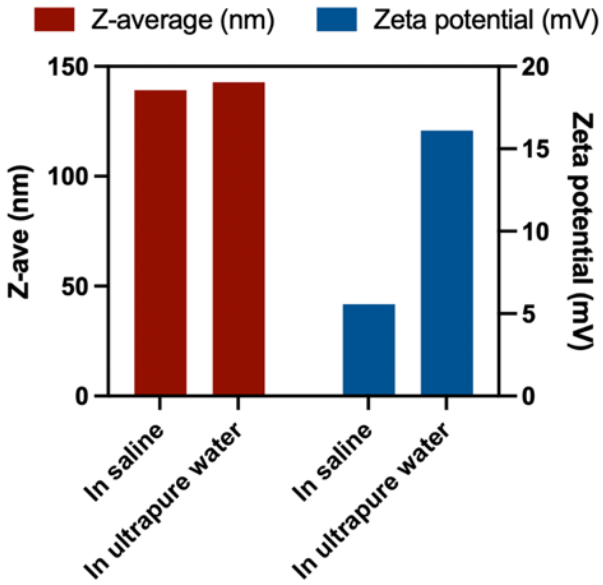

Figure 2. *The effect of using saline as rehydration solvent on decreasing surface charge of nanoparticles measured by zeta potential along with size.*

After switching the rehydration solvent to ultrapure water, a similar size was observed, while the zeta potential exhibited a significant increase. Generally, nanoparticle rehydrated in ultrapure water showed a 9.2% increase in average size, and a 2.9-fold increase in zeta potential compared to nanoparticle rehydrated in saline. This result indicated that the ions in saline solution might contribute to the change in zeta potential measurement. Besides its potential

impact in zeta potential measurement, the ions in saline solution might also disrupt with the binding of negatively charged nucleic acids molecules on positively charged nanoparticle in the next step.

3.1.3. Effect of PTX addition into nanoparticle on its average size and zeta potential

The rapidly developing vasculature of cancer tissue can result in the passive extravasation and accumulation of liposomes within tumors—an effect commonly known as the enhanced permeability and retention (EPR) effect (Matsumura et al., 1986). This phenomenon enables the circulation of nanoparticles with size smaller than 150 nm (Danaei et al., 2018). Meanwhile, some other studies stated that nanoparticle under the size of 200 nm also exhibited similar observation (Caracciolo, 2018; Maeda, 2015). Generally, nanoparticle average size should be less than 200 nm to enhance its accumulation in tumor tissues and the size of smaller than 150 nm is desired. To enable the binding of nucleic acid molecules, nanoparticle needs to be positively charged. In this section, the impact of adding PTX in nanoparticle average size and zeta potential was exhibited and discussed.

The impact of adding PTX into DG-in-LNP core formulation was studied in the same method as studying the impact of adding DOTAP into formulation. The results were shown in **Table 5** and **Figure 3**.

Table 5. Effect of loading chemotherapy drug PTX in DG-in-LNP core on nanoparticle size and surface charge along with uniformity by PDI in nanoparticle #6-9.

Nanoparticle # - (% of DOTAP)	PTX	Z-average (nm)	PDI	Zeta potential (mV)
6 (20%)	Yes	189.3	0.40	-7.4
6 (20%)	No	177.0	0.42	-8.9
7 (30%)	Yes	140.4	0.46	-6.0
7 (30%)	No	139.0	0.46	-6.7
8 (40%)	Yes	153.3	0.40	+5.7
8 (40%)	No	151.6	0.57	+5.1
9 (50%)	Yes	154.1	0.39	+9.2
9 (50%)	No	155.1	0.39	+9.0

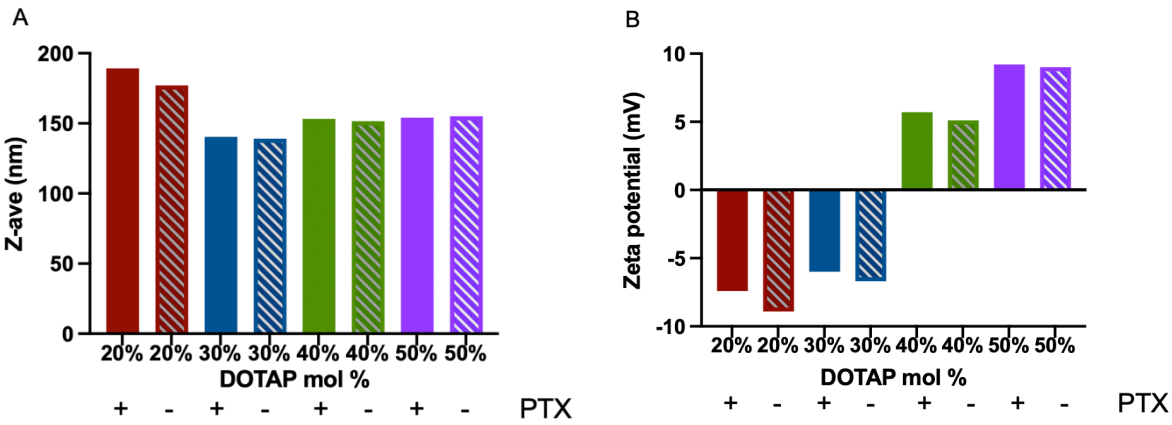

Figure 3. *The impact of loading chemotherapy drug PTX in DG-in-LNP core on nanoparticle size and surface charge along with uniformity by PDI.* ***(A)*** *The Z-average of DG-in-LNP core formulation #6-9 with or without PTX.* ***(B)*** *The zeta potential of DG-in-LNP core formulation #6-9 with or without PTX.*

Comparing the DG-in-LNP core with PTX loading the similar overall trend of increasing zeta potential in nanoparticles without PTX was observed as DOTAP molar ratio increased. An overturn of zeta potential was observed from 30% to 40% DOTAP molar ratio, which was the same as nanoparticles with PTX. In addition to the similar trend in zeta potential changes

observed for nanoparticles with and without PTX across varying DOTAP molar percentages, their zeta potentials were also comparable at equivalent DOTAP contents. This indicated that the loading of PTX in DG-in-LNP core did not have a significant impact in its zeta potential.

Meanwhile, the average nanoparticle size exhibited a decrease in average size from adding 20% DOTAP to 30% DOTAP in molar ratio and maintained the size within 10.8% range of change for the rest of formulations. While DG-in-LNP core showed the same overall trend of increasing zeta potential with increased DOTAP molar ratio, it also exhibited a similar pattern of average size and zeta potential prior to and after adding PTX. Nanoparticles except formulation #6 showed accepted average sizes of around 150 nm, which were illegible to greatly accumulate at tumor sites. Nanoparticle #6, which contained the lowest molar percent of DOTAP, had the greatest average size compared to other formulations. This unexpected observation might be induced by weak sonication during the rehydration step as the process to make nanoparticle was highly manual. Even though, its average size was still under 200 nm and did not exceed the boundary. Similar to the zeta potential comparison between nanoparticles with and without PTX, they also exhibited no significant variation in average size.

3.1.4. Impact of substituting partial structural lipid DSPC with cholesterol in nanoparticle average size and zeta potential

In section 3.1.3., the effect of nanoparticle size in its accumulation in tumor tissues was discussed. Regardless of the DOTAP molar percent and PTX loading, the average nanoparticle sizes were around or greater than 150 nm. To further enhance the circulation functionality of nanoparticle in tumor sites, its average size needed to be reduced. Cholesterol, which increases structural integrity (Kauffman et al., 2015), was added into the formulation to stabilize the DG-in-LNP core and overcome the structural fluidity introduced by DOTAP molecules. Formulations which had lower DOTAP percentage in lipid components (20% and 25%) were positively charged and had smaller size compared to formulation with high DOTAP composition. Therefore, 20% and 25% DOTAP formulation were selected to test the impact of replacing 20% of DSPC with cholesterol in DG-in-LNP core's average size and zeta potential. DG-in-LNP core formulation #10 was selected to measure the average size and zeta potential variation prior to or after adding cholesterol, and the result was in **Figure 4**.

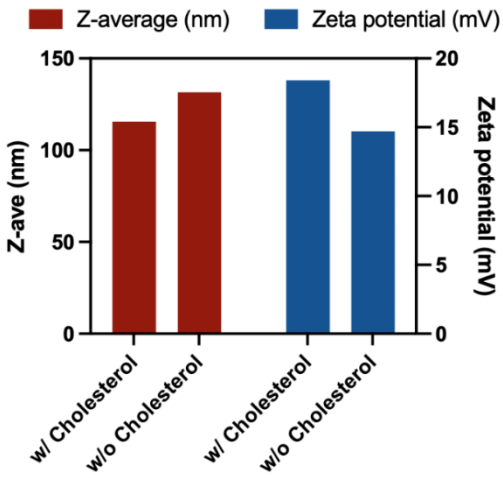

Figure 4. *The impact of substituting 20 molar % of DSPC with 20 molar % of cholesterol in DG-in-LNP lipid composition to evaluate potential size reduction and increase in surface charge by zeta potential.*

Adding cholesterol into DG-in-LNP core formulation induced a 12% reduction in average nanoparticle size. Meanwhile, a 25% increase in zeta potential was observed. This result indicated that the addition of cholesterol into formulation was able to reduce nanoparticle average size while getting more positively charged, evidencing that cholesterol had the function of stabilizing nanoparticle lipid structure.

Cholesterol was fixed at 20% of total lipid component. The average size and zeta potential measured by DLS were presented in **Table 6**.

Table 6. Effect of loading cholesterol in DG-in-LNP core on nanoparticle size reduction and increase in surface charge by zeta potential along with uniformity by PDI in nanoparticle #14 and 15.

Nanoparticle # - (% of DOTAP)	Z-average (nm)	PDI	Zeta potential (mV)
14 (20%)	111.3	0.25	+15.0
15 (25%)	115.6	0.25	+18.4

During the testing process in section 3.1, a discrepancy of zeta potential measurements was discovered between nanoparticles that contained DOTAP from different vendors (Avanti Polar Lipids and MedChemExpress). We discovered that nanoparticles prepared using DOTAP from MedChemExpress showed a higher zeta-potential comparing to DOTAP in chloroform provided by Avanti Polar Lipids. Meanwhile, the nanoparticle size did not show a significant difference between DOTAP from two vendors.

3.2. Effect of mRNA loading on nanoparticle average size and zeta potential

The DG-in-LNP core formulation #14 was selected for mRNA *in vitro* transfection because a smaller average size with moderately positive zeta potential was exhibited. In a 2015 study by Xu et al., treatment with polymeric nanoparticles co-delivering paclitaxel (PTX) and a PEDF plasmid at a weight ratio of 5:1 resulted in a 3-fold reduction in tumor weight and a median survival extension of 13 days in Balb/c mice (Xu et al., 2015). Therefore, PTX:mRNA w/w ratio of 5:1 was selected for mRNA loaded DG-in-LNP *in vitro* transfection in both 4T1 and MDA-MB-231 cells. The model gene mCherry mRNA was used to evaluate the impact of mRNA loading on nanoparticle average size and zeta potential, but the size of mCherry mRNA was considerable. As mCherry mRNA was vulnerable to degradation in cell culture medium and cell cytoplasm, negatively charged HA was used to control the charge of nanoparticle while PTX:mRNA w/w ratio of 5:1 was maintained. The impact of mCherry mRNA and HA loading on nanoparticle average size and zeta potential was measured and presented in **Table 7** and **Figure 5**.

Table 7. The Effect of loading mRNA molecules on nanoparticle surface to evaluate increase in nanoparticle size and decrease in surface charge measured by zeta potential in nanoparticle formulation #16-24.

Nanoparticle #	PTX:mRNA w/w ratio	NP:HA w/w ratio	Z-average (nm)	Zeta potential (mv)
16	5:1	N/A	1312.0	+9.6
17	5:1	40:1	1525.0	+7.5
18	5:1	10:1	2254.0	-1.4
19	5:1	7.5:1	2038.0	-2.6
20	5:1	5:1	2023.0	-9.2
21	5:1	4:1	1512.0	-6.7
22	5:1	3.5:1	2456.0	-11.5
23	5:1	3:1	113.2	-10.8
24	5:1	2.5:1	2401.0	-5.8

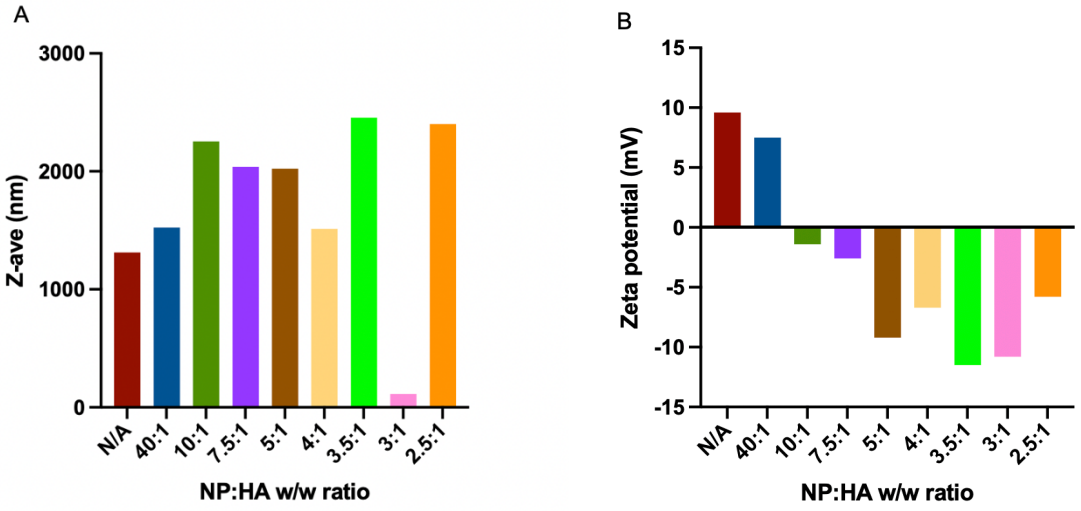

Figure 5. *Effect of loading HA molecules to evaluate increase in nanoparticle size and decrease in surface charge measured by zeta potential in mRNA loaded DG-in-LNP at a fixed PTX:mRNA*

w/w ratio of 5:1. ***(A)*** *The Z-average of DG-in-LNP core formulation #17-24.* ***(B)*** *The zeta potential of DG-in-LNP core formulation #17-24.*

From results in **Table 6** and **Figure 5**, a clear trend of decreased zeta potential and increased average nanoparticle size was observed when the amount of negatively charged compound (mRNA and HA) added onto DG-in-LNP core increased. The decrease of mRNA loaded DG-in-LNP zeta potential showed a fluctuation at nanoparticle #20 to 24, while a significant decrease in #23 average size was discovered. This was due to a measurement error. An overturn of zeta potential from positive to negative was observed between nanoparticle #17 and 18. The decrease of zeta potential indicated that the loading of negatively charged compound was able to overturn the positively charged DG-in-LNP core to negatively charged, enabling the loading of another cationic layer on the surface of mRNA to protect it from degradation. The fluctuation of zeta potential indicated the saturation of negative charge on mRNA loaded DG-in-LNP, meaning that negatively charged molecules were no longer associated to nanoparticles with NP:HA w/w ratio of 3.5:1.

However, directly pipetting mRNA into nanoparticle to form the mixture resulted in a significant increase in average size from 111.3 nm to over 1 μm, indicating that aggregation was formed. When more HA was added into the formulation until the negative charge of nanoparticle was almost saturated, an overturn of nanoparticle average size was still not observed. This indicated that the formation of aggregation might be irreversible, suggesting that the mixing of mRNA and DG-in-LNP core should be performed at a lower concentration to avoid aggregation. Another potential method to avoid aggregation was pipetting nanoparticle slowly into nanoparticle suspension while stirring it at 500 rpm (Huang et al., 2023). In mRNA *in vitro*

transfection section, the method of pipetting while stirring was applied to mRNA and HA loaded DG-in-LNP and mRNA, HA, and chitosan loaded DG-in-LNP preparation.

3.3. mRNA transfection *in vitro*

Formulation #18 was selected to test *in vitro* transfection efficiency of DG-in-LNP with (mRNA, HA loading) and (mRNA, HA, and chitosan loading). PTX was not added into nanoparticle when preparing the DG-in-LNP core to avoid cell death caused by chemotherapy drug, which would reduce the fluorescence signal of cells and lead to inaccurate measurement. The transfection of mCherry mRNA in 4T1 and MDA-MB-231 cells was both evaluated using fluorescence microscopy. For 4T1 cell transfection, the treatment groups included lipofectamine-mRNA as a positive control, cell only as a negative control, and mRNA and HA loaded DG-in-LNP where chitosan were not loaded. The results were shown in figure 8. For MDA-MB-231 cell transfection, the treatment groups included lipofectamine-mRNA as a positive control, cell only as a negative control, and mRNA, HA, and chitosan loaded DG-in-LNP. The results were shown in **Figure 6** and **Figure 7**.

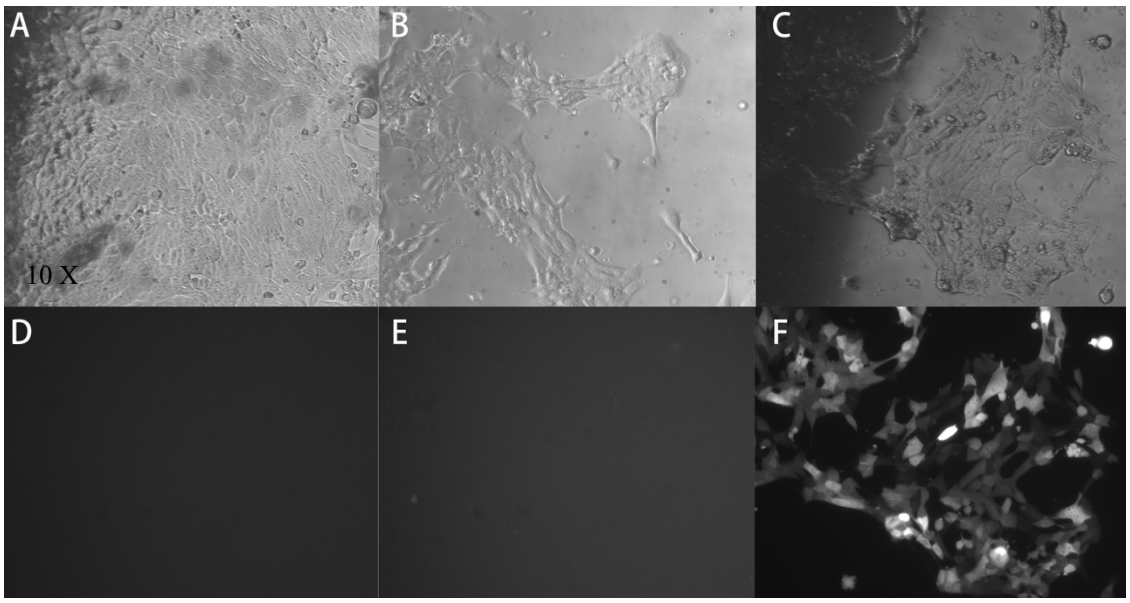

Figure 6. *The bright field and fluorescence images of negative control, mRNA and HA loaded DG-in-NP (fixed 1 μg mRNA per well), and positive control after 24 hours of incubation in 4T1 cells.* ***(A)*** *The bright field image of cell only (negative control).* ***(B)*** *The bright field image of mRNA and HA loaded DG-in-NP.* ***(C)*** *The bright field image of lipofectamine-mRNA (positive control).* ***(D)*** *The fluorescence image of cell only.* ***(E)*** *The fluorescence image of mRNA and HA loaded DG-in-LNP.* ***(F)*** *The fluorescence image of lipofectamine-mRNA. Images were captured using a 10x objective.*

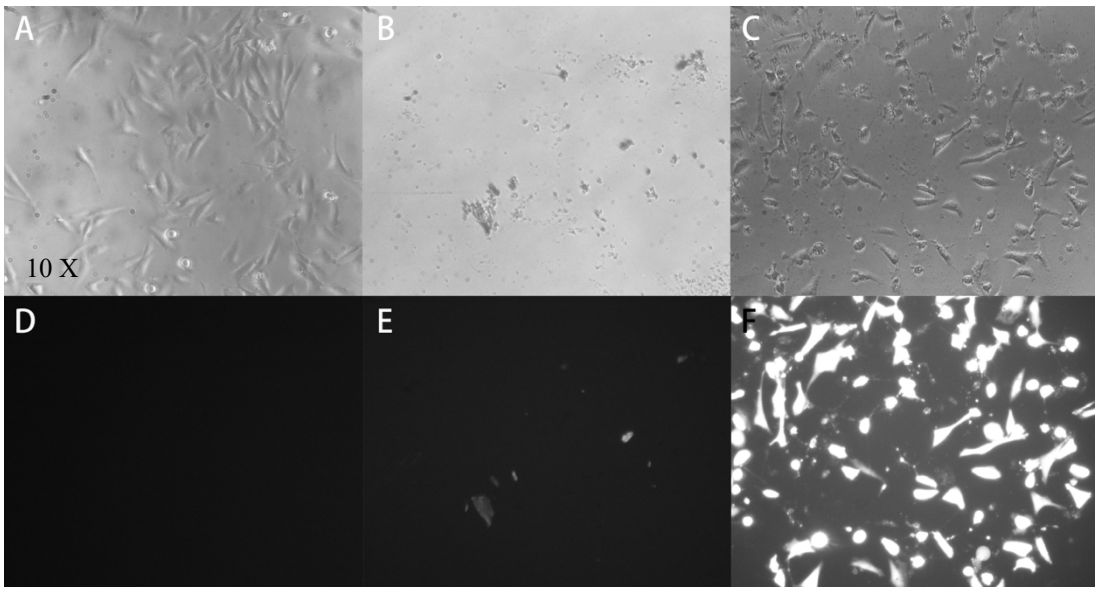

Figure 7. *The bright field and fluorescence images of negative control, mRNA and HA loaded DG-in-LNP (1 μg mRNA per well), and positive control after 24 hours of incubation in MDA-MB-231 cells.* ***(A)*** *The bright field image of cell only.* ***(B)*** *The bright field image of mRNA and HA loaded DG-in-LNP.* ***(C)*** *The bright field image of lipofectamine-mRNA.* ***(D)*** *The fluorescence image of cell only.* ***(E)*** *The fluorescence image of mRNA and HA loaded DG-in-LNP.* ***(F)*** *The fluorescence image of lipofectamine-mRNA. Images were captured using a 10x objective.*

According to **Figure 6** and **Figure 7**, an obvious fluorescence signal was observed in positive control in both 4T1 and MDA-MB-231 cells, indicating that the fluorescence microscopy and mCherry mRNA were functioning. The negative control in both cell lines exhibited no signal, meaning that there was no background noise in the measurement. However, mRNA and HA loaded DG-in-LNP in 4T1 cells showed no significant fluorescence signal. The potential reason might be low cellular uptake and degradation of mRNA in cell culture or cell cytoplasm. mRNA, HA, and chitosan loaded DG-in-NP in MDA-MB-231 cells also exhibited no significant fluorescence signal, suggesting that mRNA degradation might not intervened the expression of mCherry fluorescence protein. The result suggested that the loading of mRNA on

DG-in-LNP core surface had a high opportunity to cause aggregation and therefore prevented the nanoparticle to permeate into the cells. Therefore, siRNA, which was marked by much smaller size and more stable structure compared to mRNA, was picked to test gene loading and transfection efficiency on DG-in-LNP core using layer-by-layer method.

3.4. Effect of siRNA loading on nanoparticle average size and zeta potential

To decide the amount of siRNA loaded on nanoparticle, PTX:mRNA w/w ratios of 5:1, 2:1, and 1:1 were selected. Sams as nanoparticle mRNA loading, DG-in-LNP core formulation #14 was selected for siRNA *in vitro* transfection. The average size and zeta potential of mRNA loaded nanoparticle were presented in **Table 8** and **Figure 8**.

Table 8. The effect of loading siRNA molarecule on nanoparticle to evaluate nanoparticle size change and decrease in surface charge by zeta potential along with uniformity by PDI in nanoparticle formulation #25 to 27.

Nanoparticle #	PTX:siRNA w/w ratio	PTX	Z-average (nm)	PDI	Zeta potential (mv)
25	5:1	No	123.8	0.28	+9.7
26	2:1	Yes	124.2	0.26	+6.31
26	2:1	No	120.1	0.25	+0.99
27	1:1	Yes	128.2	0.28	-1.43
27	1:1	No	108.1	0.22	-5.6

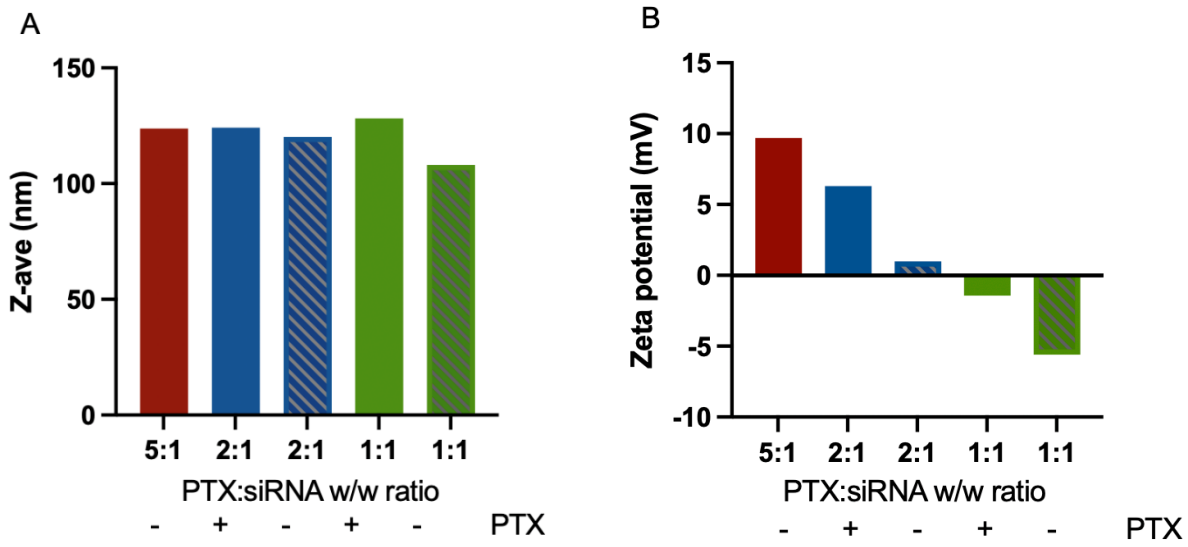

Figure 8. *The effect of loading siRNA molecules on DG-in-LNP size and surface charge.* ***(A)*** *The Z-average of DG-in-LNP core formulation #25-27.* ***(B)*** *The zeta potential of DG-in-LNP core formulation #25-27.*

From the results in **Table 8** and **Figure 10**, a trend of decreasing zeta potential was observed while the amount of siRNA loaded on nanoparticle increased, indicating that siRNA was successfully loaded on the DG-in-LNP core. An overturn of zeta potential from positive to negative was observed between nanoparticle #26 and 27. The same trend of zeta potential changes and overturn appeared in siRNA loaded nanoparticle either with or without PTX, but nanoparticle that contained PTX showed higher zeta potential generally. Meanwhile, a 10% change in average size was observed in PTX free nanoparticle loaded with varying amount of siRNA, and a similar pattern was not observed in nanoparticle with PTX. Generally, the nanoparticle average size was maintained regardless of amount of siRNA added and was below 150 nm.

Formulation #27 was selected for chitosan loading based on siRNA loaded DG-in-LNP since negatively charged mixture was needed to enable electrostatic interaction between siRNA

loaded DG-in-LNP mixture and chitosan. The loading of chitosan was based on siRNA:CHI w/w ratio as listed in table 9. The results were presented in **Table 9 and Figure 9**.

Table 9. Effect of loading chitosan on siRNA loaded nanoparticle to evaluate nanoparticle size change and increase in surface charge by zeta potential along with uniformity by PDI in nanoparticle formulation #28-31.

Nanoparticle #	PTX:siRNA:CHI w/w ratio	PTX	Z-average (nm)	PDI	Zeta potential (mv)
28	1:1:1	Yes	120.8	0.25	+0.40
28	1:1:1	No	119.4	0.15	+0.22
29	1:1:2	Yes	120.9	0.23	+2.06
29	1:1:2	No	137.6	0.19	-0.31
30	1:1:5	Yes	122.00	0.24	-0.46
30	1:1:5	No	149.1	0.20	+1.75
31	1:1:10	Yes	125.2	0.25	+3.6
31	1:1:10	No	169.0	0.32	+3.96

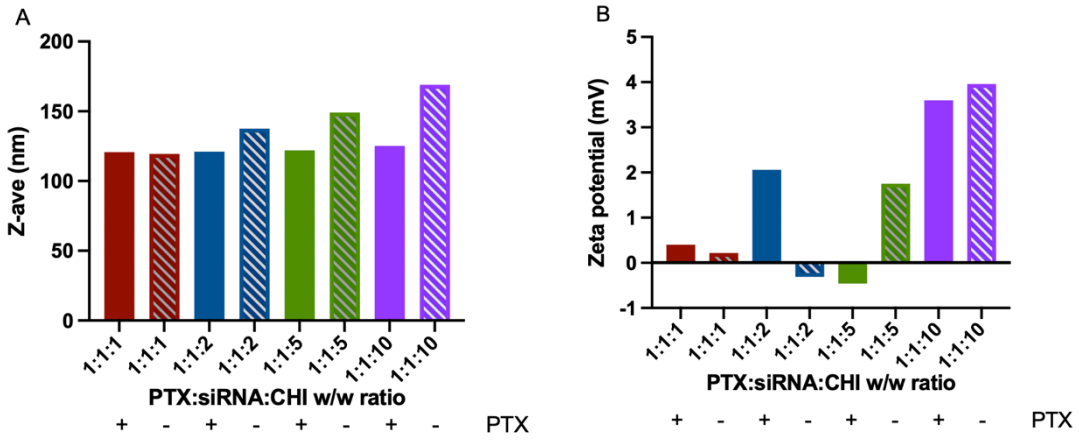

Figure 9. *Effect of loading chitosan on siRNA-loaded DG-in-LNP size and surface charge.* ***(A)*** *The Z-average of DG-in-LNP core formulation #28-31.* ***(B)*** *The zeta potential of DG-in-LNP core formulation #28-31.*

From the results in **Table 9** and **Figure 9**, a trend of increased average DG-in-LNP size was observed in PTX free siRNA loaded DG-in-LNP with increasing chitosan coating, while the size of PTX loaded DG-in-LNP did not present a significant change in average size. The increase in size observed in PTX free DG-in-LNP explained that the loading of chitosan on negatively charged DG-in-LNP mixture would lead to an increase in size. HEPEs buffer, which stabilizes the pH of solution and minimizes the particle aggregation, were added to enable the characterization of nanoparticle. The dilution of DG-in-LNP mixture from HEPEs buffer might be the reason that size changes was not observed in nanoparticle with PTX. The procedure of preparing size and zeta potential measurement was highly manual, which had opportunities to cause errors. At PTX:siRNA:CHI w/w ratio of 1:1:1, a slight positive zeta potential was observed in DG-in-LNP either with or without PTX loading, and an obvious positive zeta potential was observed in DG-in-LNP at w/w ratio of 1:1:10. At other w/w ratios between 1:1:1 and 1:1:10, a fluctuation of zeta potential was observed. The reason behind this was that DG-in-LNP mixture was nearly neutral around these ratios, therefore leading to the fluctuation in

measurement. However, the overall trend of increasing zeta potential with increased chitosan loading indicated the successful loading of chitosan on nanoparticles. Generally, all DG-in-LNP with siRNA and chitosan loading or only siRNA loading formulations at lower chitosan loading ratio had average size of less than 150 nm, while DG-in-LNP at PTX:siRNA:CHI w/w ratio of 1:1:5 and 1:1:10 without PTX showed the average size around 150 nm. In a study performed by Zhang et al. in 2020, lipid-based nanoparticle that co-delivered VEGF siRNA and PTX reached the size of 172.37 nm but still achieved a 2-fold decrease in VEGF expression (Zhang et al., 2020). This indicated that the size of our DG-in-LNP was not expected to cause any problems.

3.5. siRNA transfection *in vitro*

Formulation #25-31 (except # 28) was selected to evaluate firefly-siLuc transfection in MDA-MB-231-Luc cells. Treatment groups included lipofectamine-siRNA and free PTX at 0.34, 0.68, and 1.71 μg/mL as positive controls, cell only as a negative control, siRNA loaded DG-in-LNP, and siRNA and chitosan loaded DG-in-LNP. Alamar blue assay was performed to evaluate the cell viability after administered with same treatment groups listed above. The percentage of luminescence signal normalized with cell viability was the parameter to evaluate transfection efficiency. The reading of bioluminescence from plate reader and cell viability of each treatment group were presented in **Figure 10**.

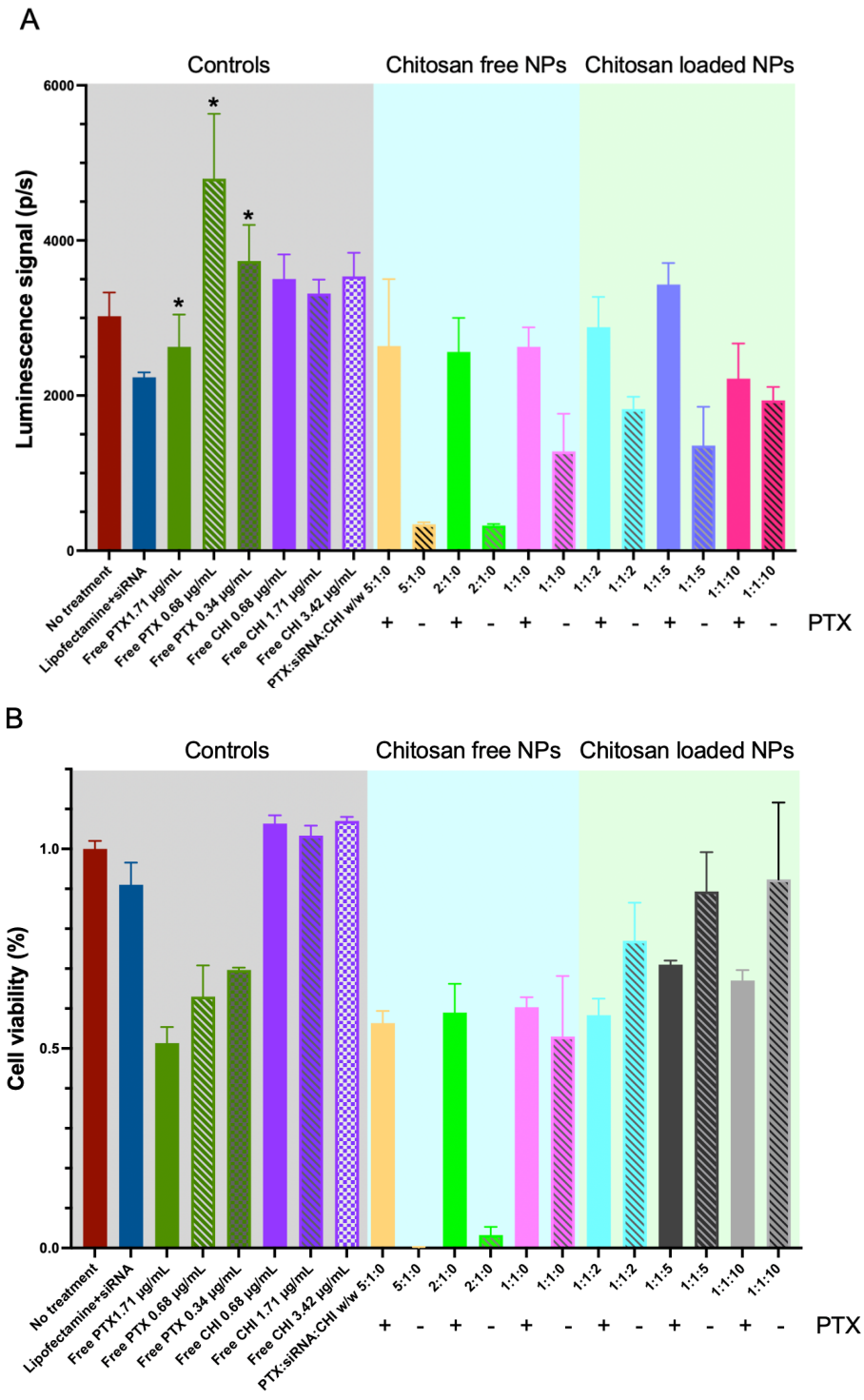

Figure 10. *Cellular luminescence* ***(A)*** *and viability* ***(B)*** *after various treatments in MDA-MB-231-Luc cells. Bars marked with * represented statistical significance ($p < 0.05$) between treated and no treatment groups.*

We discovered that free PTX at the concentration of 0.34, 0.68, and 1.71 μg/mL showed 60%, 80%, and 160% higher luminescence signal compared to no treatment after normalization by cell viability (P-value = 0.005, 0.02, and 0.008). Meanwhile, a 10% increase in luminescence signal was induced by free chitosan at PTX:siRNA:CHI ratio 1:1:2, 1:1:5, and 1:1:10 (Free Chi at 0.68, 1.71, and 3.42 μg/mL). In siRNA loaded DG-in-LNP, and siRNA and chitosan loaded DG-in-LNP treatments, notably, PTX free siRNA loaded DG-in-LNP at PTX:siRNA:CHI w/w ratio of 5:1:0 and 2:1:0 showed an extremely low luminescence signal.

PTX free nanoparticle at PTX:siRNA:CHI w/w ratio of 5:1:0 and 2:1:0 showed an extremely low cell viability of only 0.08 and 3.26%, respectively. As the cell viability results were consistent, we assumed that the low cell viability was not due to experimental errors at cell seeding step, which could lead to an inconsistent cell viability reading. Instead, high toxicity of PTX free nanoparticle at PTX:siRNA:CHI w/w ratio of 5:1:0 and 2:1:0 was more likely the reason inducing low cell viability. A 91% viability was observed in lipofectamine-siRNA treatment, and 53% viability was observed in PTX free nanoparticle at PTX:siRNA:CHI w/w ratio of 1:1:0. An increasing trend of cell viability was observed when the loading of chitosan increased. The cell viability increased to 77%, 89%, and 92% when the chitosan loading increased to ratios of 1:1:2, 1:1:5, and 1:1:10, respectively. This indicated that the addition of chitosan into lipid-based nanoparticle at a higher amount could reduce the toxicity induced by nanoparticle. The cell viability in PTX loaded nanoparticle at PTX:siRNA:CHI w/w ratio of 1:1:2, 1:1:5, and 1:1:10 were 58%, 71%, and 67%, where cell viability in PTX free nanoparticle at same ratios were 77%, 89%, and 92%. The significant difference in cell viability between PTX loaded and PTX free nanoparticle indicated that PTX were released into the cells and led to cell death. However, cell viability in PTX loaded nanoparticle at PTX:siRNA:CHI w/w ratio of 1:1:0

was 61%, while cell viability in PTX free nanoparticle at same ratio was 53%, and a significant difference was not observed. Meanwhile, the extremely low cell viability in PTX free nanoparticle at PTX:siRNA:CHI w/w ratio at 5:1:0 and 2:1:0 were considered outliers. Therefore, more studies regarding the effect of higher nanoparticle concentration in cell viability needed to be done to conclude if nanoparticle without chitosan showed a poorer PTX release profile. The results of all secondary analysis were presented in **Figure 11**.

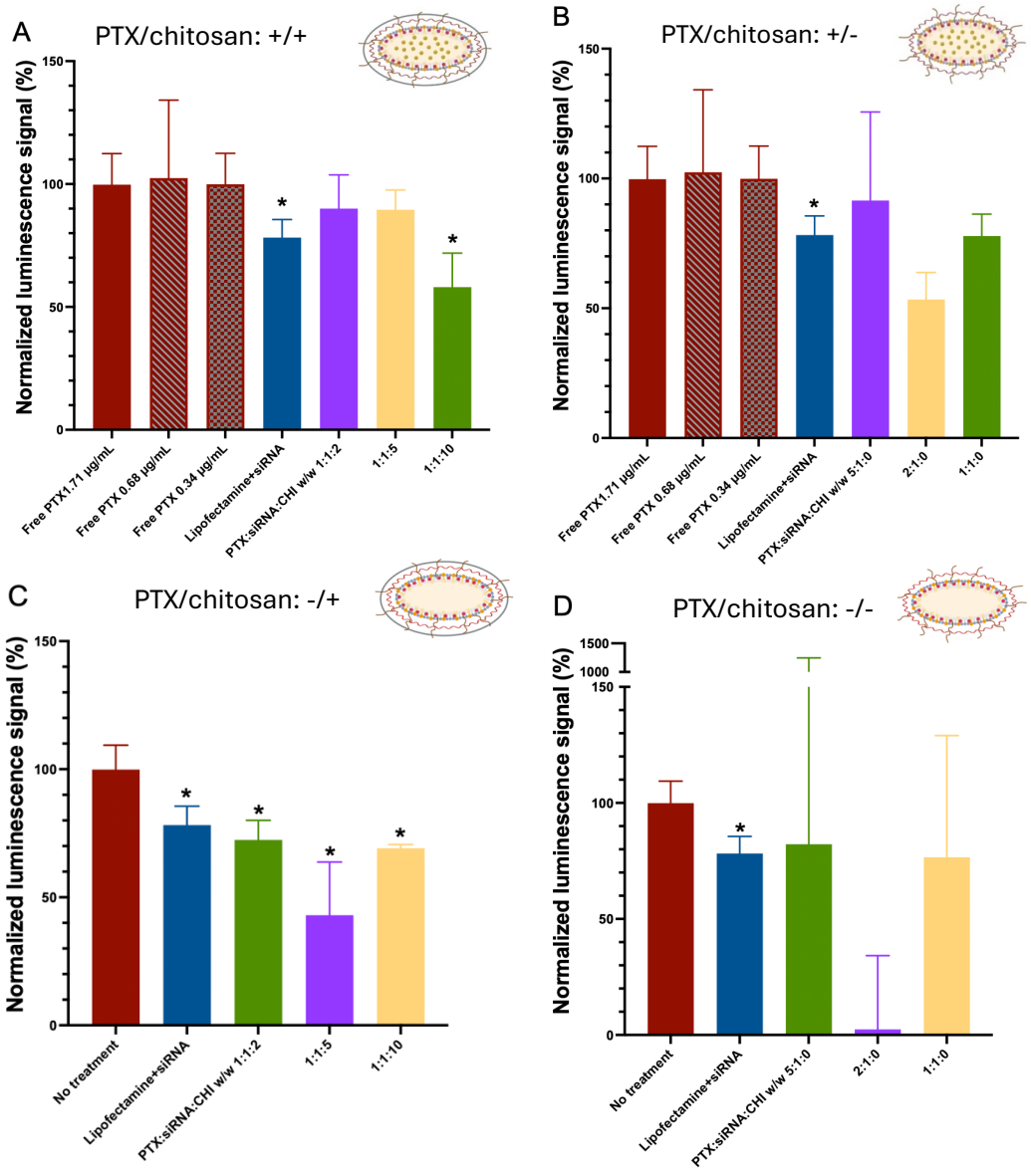

Figure 11. *Normalized luminescence signal in controls and treatments in MDA-MB-231-Luc cells (0.53 µg of siRNA was fixed per well).* ***(A)*** *Luminescence signal of nanoparticle loaded with PTX and chitosan.* ***(B)*** *Luminescence signal of nanoparticle loaded with PTX and without chitosan.* ***(C)*** *Luminsecence signal of PTX free nanoparticle loaded with chitosan.* ***(D)*** *Luminescence signal of PTX free nanoparticle without chitosan loading. Bars marked with * represented statistical significance ($p < 0.05$) between treatment and corresponding control groups (Free PTX in A and B, No treatment in C and D).*

The variation in cell viability would lead to different amount of luciferase expression between control and treatments, leading to an inaccurate siRNA transfection efficiency evaluated by luminescence signal. Therefore, luminescence signal reduction prior to normalization was not enough to evaluate the efficiency of each formulation. To enable a secondary analysis, luminescence signal of all treatments was normalized by cell viability Luminescence signal of each treatment was divided by corresponding cytotoxicity to elucidate the impact of cell viability in luminescence signal. For PTX free treatments, luminescence signal after divided by cell viability was compared with the luminescence signal of free PTX with corresponding concentration. For PTX loaded treatments, luminescence signal after divided by cell viability was compared with no treatment. Lipofectamine+siRNA result was normalized following the same method as PTX free treatments.

After normalizing luminescence signal with cell viability, a 22% decrease in luminescence signal was observed in lipofectamine-siRNA (P-value = 0.04). In panel (D), an extremely low luminescence signal % was discovered in PTX free DG-in-LNP at PTX:siRNA:CHI w/w ratio of 2:1:0. However, a low cell viability of PTX free DG-in-LNP at PTX:siRNA:CHI w/w ratio of 2:1:0 was also reported in figure 10 (B), suggesting that the result was not statistically significant due to its extreme values in luminescence signal and cell viability. In PTX and chitosan loaded DG-in-LNP, PTX:siRNA:CHI w/w ratio of 1:1:10 showed a 40% luminescence signal reduction (P-value = 0.02), while PTX:siRNA:CHI w/w ratio of 1:1:2 and 1:1:5 did not show any significant signal reduction. PTX free but chitosan loaded DG-in-LNP at PTX:siRNA:CHI w/w ratio of 1:1:2, 1:1:5, and 1:1:10 showed luminescence signal reduction of 30%, 60%, and 30% (P-value = 0.02, 0.01, 0.005), indicating that siRNA has been successfully delivered and transfected in MDA-MB-231-Luc cells. The significantly higher

luminescence signal in PTX loaded DG-in-LNP at PTX:siRNA:CHI w/w ratio of 1:1:2 and 1:1:5 might be induced by the microtubule arresting function of PTX (Abu Samaan et al., 2022). Microtubule serves to move the endosome after endocytosis, and PTX might prevent the release of siRNA to targeted destination. This resulted in a higher luminescence signal since fewer amounts of siLuc were delivered into the cells. DG-in-LNP that carried PTX should be further studied to investigate if siRNA delivery was hindered by adding PTX into formulation. PTX loaded DG-in-LNP at PTX:siRNA:CHI w/w ratio of 1:1:10 achieved luminescence signal reduction of 40% was compared to luminescence signal reduction of 30% in PTX free nanoparticle at same w/w ratio. This result suggested that loading of chitosan at PTX:siRNA:CHI w/w ratio of 1:1:10 had eliminated the signal reduction difference bewteen PTX loaded and PTX free nanoparticles. This discovery might explain that increased loading of chitosan could potentially overcome the retardation of siRNA delivery induced by PTX and led to a synergistic effect of increased siRNA delivery while PTX was also released into the cells. The similar trend was not discovered in DG-in-LNP at lower PTX:siRNA:CHI w/w ratio. These findings suggested that 1) PTX free DG-in-LNP with chitosan loading showed efficacy in delivering siRNA. 2) PTX loading in DG-in-LNP could hinder the siRNA delivery in nanoparticle. 3) chitosan loading at a higher ratio could overturn the hindrance of PTX in siRNA delivery and showed efficacy in TNBC cell knockout.

In a study performed in 2020, Zhang et al. reported a lipid nanoparticle to co-deliver VEGF siRNA and PTX against non-small lung cancer (Zhang et al., 2020). While a LbL approach was used to load siRNA on nanoparticle, the zeta potential of nanoparticles was over +50 mV. Meanwhile, the nanoparticle size reported by Zhang et al. exceeded 150 nm. In our study, DG-in-LNP size was smaller than 150 nm, but zeta potential was less than +10 mV.

Nanoparticle co-delivering PTX and VEGF siRNA showed 80% reduction in VEGF expression in NCI-H460 cells, which had high efficacy (Zhang et al., 2020). In a study performed by Jiang et al. in 2011, cationic nanoparticle showed a 4-fold higher cellular uptake in mesenchymal stem cells compared to anionic nanoparticle (Jiang et al., 2011). Similar conclusion was stated in some other studies (Villanueva et al., 2009; Thorek et al., 2008). These studies might suggest that nanoparticle with higher positive charges might be more effective in co-delivering PTX and siRNA molecules. Positive charged molecules might cause extra cytotoxicity, although nanoparticle with greater positive charge should be studied to test if extra positive charge can enhance the delivery of nucleic acid molecules into cells due to its increased cellular uptake (Fröhlich, 2012). Therefore, DG-in-LNP with chitosan loading higher than PTX:siRNA:CHI w/w ratio of 1:1:10 needed to be further studied to validate the explanation of positive charge effect in cellular uptake.

4. CONCLUSION

Building on an innovative approach to co-deliver highly potent chemotherapeutic drug PTX, and a nucleic acid polymer, siRNA, that may interfere at gene expression levels on tumor growth, this thesis research has designed, optimized and characterized drug-gene combination built into a lipid-nanoparticle platform. To do so, a LbL approach was applied to load a layer of negatively charged RNA polymers on positively charged DG-in-LNP core, and another layer of positively charged polymer chitosan on the layer of RNA polymer. In this way, the LbL structured DG-in-LNP structure could achieve a more consistent and sustained release of PTX and RNA molecules into TNBC cells. To be specific, positively charged DG-in-LNP cores with

PTX were allowed to coat with mRNA or siRNA negatively charged polymer to provide drug-gene carrier. The remaining net charges on DG-in-LNP were neutralized or stabilized with chitosan, a positively charge polymer enhancing nanoparticle stability, cellular uptake, and sustained release of therapeutics in nanoparticle. The studies have shown that siRNA and PTX can be made stable into a single DG-in-LNP platform. In vitro, a 2-fold enhanced suppression of TNBC cell growth was noted with PTX loaded DG-in-LNP. Meanwhile, a trend of increasing cell viability was observed in PTX free DG-in-LNP with higher amount of chitosan loading. Additional analysis revealed that a 40% reduction in luminescence signal was observed in PTX loaded DG-in-LNP carrying siLuc that induced the knockdown of luciferase protein in MDA-MB-231- Luc cells at PTX:siRNA:CHI w/w ratio of 1:1:10, showing a satisfactory efficacy in siRNA transfection. Meanwhile, PTX loaded DG-in-LNP at PTX:siRNA:CHI w/w ratio of 1:1:2 and 1:1:5 showed much lower signal reduction efficiency compared to PTX free DG-in-LNP at same PTX:siRNA:CHI w/w ratio. The result indicated the potential hindrance of siRNA delivery caused by PTX loading. However, the variation in luminescence signal reduction efficacy was eliminated in DG-in-NP at PTX:siRNA:CHI w/w ratio of 1:1:10, suggesting that higher amount of chitosan loading could overcome the hindrance of PTX in siRNA transfection.

Future studies may need to explore the increase in luminescence signal when cells were treated with PTX, and that would explain if PTX prevent the endosomal escape of siRNA from nanocarriers. The effect of chitosan in siRNA delivery should also be studied at higher chitosan loading content to confirm if a synergistic effect is induced. In addition, nucleic acids binding studies may be needed to further characterize the loading capacity of the nanoparticle. The cellular uptake studies of nanoparticle were also needed to further evaluate the efficiency of nanoparticle. siLuc can be substituted with therapeutic siRNA, such as proline-, glutamic acid-,

and leucine-rich protein 1 (PELP1) siRNA. PELP1 is a scaffold protein with enzyme activity shown in TNBC (Altwegg et al., 2023). PELP1 siRNA had similar structure with siLuc, including its size and charge, and was expected to be substituted by siLuc without complicated formulation modification. By substituting siLuc with PELP1 siRNA, the knockout efficiency of TNBC cells with PELP1 and PTX co-loaded DG-in-LNP could be evaluated, and the presence or absence of synergestic effects can be studied.

This study provided significant understanding into the impact of substituting structural lipids with cationic lipid and cholesterol on nanoparticle physical and chemical properties and offered an insight to understand the function of chitosan in LbL prepared DG-in-LNP. Lastly, this study contributed to a nanoparticle formulation which enabled the simultaneous delivery of siRNA and PTX against human TNBC cells and showed efficacy against tumor cell growth. Future studies should further explore the relationship between nanoparticle concentration and cell viability, while PTX in siRNA delivery hindrance should also be studied. To explore nanoparticle with greater efficacy, a higher chitosan loading in nanoparticle should also be tested.

5. REFERENCES

(1) Abu Samaan, T.; Samec, M.; Liskova, A.; Kubatka, P.; Büsselberg, D. Paclitaxel's Mechanistic and Clinical Effects on Breast Cancer. *BIOMOLECULES* **2019**, *9* (12). DOI: 10.3390/biom9120789.

(2) Aliabadi, H.; Maranchuk, R.; Kucharski, C.; Mahdipoor, P.; Hugh, J.; Uludag, H. Effective response of doxorubicin-sensitive and -resistant breast cancer cells to combinational siRNA therapy. *JOURNAL OF CONTROLLED RELEASE* **2013**, *172* (1), 219-228. DOI: 10.1016/j.jconrel.2013.08.012.

(3) Alkekhia, D.; Hammond, P.; Shukla, A. Layer-by-Layer Biomaterials for Drug Delivery. In *ANNUAL REVIEW OF BIOMEDICAL ENGINEERING, VOL 22*, 2020; Vol. 22, pp 1-24.

(4) Altwegg, K.; Pratap, U.; Liu, Z.; Liu, J.; Sanchez, J.; Yang, X.; Ebrahimi, B.; Panneerdoss, D.; Li, X.; Sareddy, G.; et al. Targeting PELP1 oncogenic signaling in TNBC with the small molarecule inhibitor SMIP34. *BREAST CANCER RESEARCH AND TREATMENT* **2023**, *200* (1), 151-162. DOI: 10.1007/s10549-023-06958-4.

(5) Caracciolo, G. Clinically approved liposomal nanomedicines: lessons learned from the biomolarecular corona. *NANOSCALE* **2018**, *10* (9), 4167-4172. DOI: 10.1039/c7nr07450f.

(6) Chen, I.; Lin, C.; Huang, C.; Lien, H.; Hsu, C.; Kuo, W.; Lu, Y.; Cheng, A. Lack of efficacy to systemic chemotherapy for treatment of metaplastic carcinoma of the breast in the modern era. *BREAST CANCER RESEARCH AND TREATMENT* **2011**, *130* (1), 345-351. DOI: 10.1007/s10549-011-1686-9.

(7) Cocco, S.; Leone, A.; Roca, M.; Lombardi, R.; Piezzo, M.; Caputo, R.; Ciardiello, C.; Costantini, S.; Bruzzese, F.; Sisalli, M.; et al. Inhibition of autophagy by chloroquine prevents resistance to PI3K/AKT inhibitors and potentiates their antitumor effect in combination with paclitaxel in triple negative breast cancer models. *JOURNAL OF TRANSLATIONAL MEDICINE* **2022**, *20* (1), Article. DOI: 10.1186/s12967-022-03462-z.

(8) Cortes, J.; Cescon, D.; Rugo, H.; Nowecki, Z.; Im, S.; Yusof, M.; Gallardo, C.; Lipatov, O.; Barrios, C.; Holgado, E.; et al. Pembrolizumab plus chemotherapy versus placebo plus chemotherapy for previously untreated locally recurrent inoperable or metastatic triple-negative breast cancer (KEYNOTE-355): a randomised, placebo-controlled, double-blind, phase 3 clinical trial. *LANCET* **2020**, *396* (10265), 1817-1828, Article.

(9) Danaei, M.; Dehghankhold, M.; Ataei, S.; Davarani, F.; Javanmard, R.; Dokhani, A.; Khorasani, S.; Mozafari, M. Impact of Particle Size and Polydispersity Index on the Clinical

Applications of Lipidic Nanocarrier Systems. *PHARMACEUTICS* **2018**, *10* (2). DOI: 10.3390/pharmaceutics10020057.

(10) Dasari, S.; Tchounwou, P. Cisplatin in cancer therapy: Molarecular mechanisms of action. *EUROPEAN JOURNAL OF PHARMACOLOGY* **2014**, *740*, 364-378. DOI: 10.1016/j.ejphar.2014.07.025.

(11) Deng, Z.; Morton, S.; Ben-Akiva, E.; Dreaden, E.; Shopsowitz, K.; Hammond, P. Layer-by-Layer Nanoparticles for Systemic Codelivery of an Anticancer Drug and siRNA for Potential Triple-Negative Breast Cancer Treatment. *ACS NANO* **2013**, *7* (11), 9571-9584. DOI: 10.1021/nn4047925.

(12) Fröhlich, E. The role of surface charge in cellular uptake and cytotoxicity of medical nanoparticles. *INTERNATIONAL JOURNAL OF NANOMEDICINE* **2012**, *7*, 5577-5591. DOI: 10.2147/IJN.S36111.

(13) Gavrilov, K.; Saltzman, W. M. Therapeutic siRNA: principles, challenges, and strategies. *The Yale journal of biology and medicine* **2012**, *85* (2), 187-200.

(14) Gradishar, W. J.; Moran, M. S.; Abraham, J.; Abramson, V.; Aft, R.; Agnese, D.; Allison, K. H.; Anderson, B.; Bailey, J.; Burstein, H. J.; et al. NCCN Clinical Practice Guideline in Oncology for Breast Cancer. National Comprehension Cancer Network: 2025.

(15) Gupta, A.; Andresen, J.; Manan, R.; Langer, R. Nucleic acid delivery for therapeutic applications. *ADVANCED DRUG DELIVERY REVIEWS* **2021**, *178*. DOI: 10.1016/j.addr.2021.113834.

(16) HAENSLER, J.; SZOKA, F. POLYAMIDOAMINE CASCADE POLYMERS MEDIATE EFFICIENT TRANSFECTION OF CELLS IN CULTURE. *BIOCONJUGATE CHEMISTRY* **1993**, *4* (5), 372-379. DOI: 10.1021/bc00023a012.

(17) Hu, B.; Zhong, L.; Weng, Y.; Peng, L.; Huang, Y.; Zhao, Y.; Liang, X. Therapeutic siRNA: state of the art. *SIGNAL TRANSDUCTION AND TARGETED THERAPY* **2020**, *5* (1). DOI: 10.1038/s41392-020-0207-x.

(18) Hu, Q.; Chen, W.; Zhong, S.; Li, J.; Luo, Z.; Tang, J.; Zhao, J. Current Progress in the Treatment of Metaplastic Breast Carcinoma. *ASIAN PACIFIC JOURNAL OF CANCER PREVENTION* **2013**, *14* (11), 6221-6225, Review. DOI: 10.7314/APJCP.2013.14.11.6221.

(19) Huang, J.; Lin, G.; Juenke, T.; Chung, S.; Lai, N.; Zhang, T.; Zhang, T.; Zhang, M. Iron Oxide Nanoparticle-Mediated mRNA Delivery to Hard-to-Transfect Cancer Cells. *PHARMACEUTICS* **2023**, *15* (7). DOI: 10.3390/pharmaceutics15071946.

(20) Jaaks, P.; Coker, E.; Vis, D.; Edwards, O.; Carpenter, E.; Leto, S.; Dwane, L.; Sassi, F.; Lightfoot, H.; Barthorpe, S.; et al. Effective drug combinations in breast, colon and pancreatic cancer cells. *NATURE* **2022**, *603* (7899), 166-+. DOI: 10.1038/s41586-022-04437-2.

(21) Jacob, E.; Huang, J.; Chen, M. Lipid nanoparticle-based mRNA vaccines: a new frontier in precision oncology. *PRECISION CLINICAL MEDICINE* **2024**, *7* (3). DOI: 10.1093/pcmedi/pbae017.

(22) Jafernik, K.; Ladniak, A.; Blicharska, E.; Czarnek, K.; Ekiert, H.; Wiacek, A.; Szopa, A. Chitosan-Based Nanoparticles as Effective Drug Delivery Systems-A review. *MOLECULES* **2023**, *28* (4). DOI: 10.3390/molecules28041963.

(23) Jiang, T.; Zhu, J.; Jiang, S.; Chen, Z.; Xu, P.; Gong, R.; Zhong, C.; Cheng, Y.; Sun, X.; Yi, W.; et al. Targeting lncRNA DDIT4-AS1 Sensitizes Triple Negative Breast Cancer to Chemotherapy via Suppressing of Autophagy. *ADVANCED SCIENCE* **2023**, *10* (17). DOI: 10.1002/advs.202207257.

(24) Jiang, X.; Musyanovych, A.; Röcker, C.; Landfester, K.; Mailänder, V.; Nienhaus, G. Specific effects of surface carboxyl groups on anionic polystyrene particles in their interactions with mesenchymal stem cells. *NANOSCALE* **2011**, *3* (5), 2028-2035. DOI: 10.1039/c0nr00944j.

(25) Karikó, K.; Buckstein, M.; Ni, H.; Weissman, D. Suppression of RNA recognition by Toll-like receptors:: The impact of nucleoside modification and the evolutionary origin of RNA. *IMMUNITY* **2005**, *23* (2), 165-175. DOI: 10.1016/j.immuni.2005.06.008.

(26) Kauffman, K.; Dorkin, J.; Yang, J.; Heartlein, M.; DeRosa, F.; Mir, F.; Fenton, O.; Anderson, D. Optimization of Lipid Nanoparticle Formulations for mRNA Delivery in Vivo with Fractional Factorial and Definitive Screening Designs. *NANO LETTERS* **2015**, *15* (11), 7300-7306. DOI: 10.1021/acs.nanolett.5b02497.

(27) Kim, Y.; Choi, J.; Kim, E.; Park, W.; Jang, H.; Jang, Y.; Chi, S.; Kweon, D.; Lee, K.; Kim, S.; et al. Design of PD-L1-Targeted Lipid Nanoparticles to Turn on PTEN for Efficient Cancer Therapy. *ADVANCED SCIENCE* **2024**, *11* (22). DOI: 10.1002/advs.202309917.

(28) Klar, N.; Rosenzweig, M.; Diergaarde, B.; Brufsky, A. Features Associated With Long-Term Survival in Patients With Metastatic Breast Cancer. *CLINICAL BREAST CANCER* **2019**, *19* (4), 304-310. DOI: 10.1016/j.clbc.2019.01.014.

(29) Kotterman, M.; Schaffer, D. Engineering adeno-associated viruses for clinical gene therapy. *NATURE REVIEWS GENETICS* **2014**, *15* (7), 445-451. DOI: 10.1038/nrg3742.

(30) Li, Y.; Chen, Y.; Li, J.; Zhang, Z.; Huang, C.; Lian, G.; Yang, K.; Chen, S.; Lin, Y.; Wang, L.; et al. Co-delivery of microRNA-21 antisense oligonucleotides and gemcitabine using nanomedicine for pancreatic cancer therapy. *CANCER SCIENCE* **2017**, *108* (7), 1493-1503. DOI: 10.1111/cas.13267.

(31) Libson, S.; Lippman, M. A review of clinical aspects of breast cancer. *INTERNATIONAL REVIEW OF PSYCHIATRY* **2014**, *26* (1), 4-15, Article. DOI: 10.3109/09540261.2013.852971.

(32) Liedtke, C.; Mazouni, C.; Hess, K.; Andre, F.; Tordai, A.; Mejia, J.; Symmans, W.; Gonzalez-Angulo, A.; Hennessy, B.; Green, M.; et al. Response to neoadjuvant therapy and long-term survival in patients with triple-negative breast cancer. *JOURNAL OF CLINICAL ONCOLOGY* **2008**, *26* (8), 1275-1281. DOI: 10.1200/JCO.2007.14.4147.

(33) Liu, C.; Shi, Q.; Huang, X.; Koo, S.; Kong, N.; Tao, W. mRNA-based cancer therapeutics. *NATURE REVIEWS CANCER* **2023**, *23* (8), 526-543. DOI: 10.1038/s41568-023-00586-2.

(34) Longley, D.; Harkin, D.; Johnston, P. 5-Fluorouracil: Mechanisms of action and clinical strategies. *NATURE REVIEWS CANCER* **2003**, *3* (5), 330-338. DOI: 10.1038/nrc1074.

(35) Maeda, H. Toward a full understanding of the EPR effect in primary and metastatic tumors as well as issues related to its heterogeneity. *ADVANCED DRUG DELIVERY REVIEWS* **2015**, *91*, 3-6. DOI: 10.1016/j.addr.2015.01.002.

(36) Panalytical, M. *Manual: Zetasizer Nano User Manual (Man0485-1.1)*; 2013.

(37) Markman, J.; Rekechenetskiy, A.; Holler, E.; Ljubimova, J. Nanomedicine therapeutic approaches to overcome cancer drug resistance. *ADVANCED DRUG DELIVERY REVIEWS* **2013**, *65* (13-14), 1866-1879. DOI: 10.1016/j.addr.2013.09.019.

(38) Marra, A.; Curigliano, G. Adjuvant and Neoadjuvant Treatment of Triple-Negative Breast Cancer With Chemotherapy. *CANCER JOURNAL* **2021**, *27* (1), 41-49. DOI: 10.1097/PPO.0000000000000498.

(39) MATSUMURA, Y.; MAEDA, H. A NEW CONCEPT FOR MACROMOLARECULAR THERAPEUTICS IN CANCER-CHEMOTHERAPY - MECHANISM OF TUMORITROPIC ACCUMULATION OF PROTEINS AND THE ANTITUMOR AGENT SMANCS. *CANCER RESEARCH* **1986**, *46* (12), 6387-6392.

(40) Mattioli, R.; Ilari, A.; Colotti, B.; Mosca, L.; Fazi, F.; Colotti, G. Doxorubicin and other anthracyclines in cancers: Activity, chemoresistance and its overcoming. *MOLARECULAR ASPECTS OF MEDICINE* **2023**, *93*. DOI: 10.1016/j.mam.2023.101205.

(41) Meisel, J.; Gokel, G. A Simplified Direct Lipid Mixing Lipoplex Preparation: Comparison of Liposomal-, Dimethylsulfoxide-, and Ethanol-Based Methods. *SCIENTIFIC REPORTS* **2016**, *6*. DOI: 10.1038/srep27662.

(42) Miles, D.; Gligorov, J.; André, F.; Cameron, D.; Schneeweiss, A.; Barrios, C.; Xu, B.; Wardley, A.; Kaen, D.; Andrade, L.; et al. Primary results from IMpassion131, a double-blind, placebo-controlled, randomised phase III trial of first-line paclitaxel with or without atezolizumab for unresectable locally advanced/metastatic triple-negative breast cancer. *ANNALS OF ONCOLOGY* **2021**, *32* (8), 994-1004. DOI: 10.1016/j.annonc.2021.05.801.

(43) Moukhtari, S.; Garbayo, E.; Amundarain, A.; Pascual-Gil, S.; Carrasco-Leon, A.; Prosper, F.; Agirre, X.; Blanco-Prieto, M. Lipid nanoparticles for siRNA delivery in cancer treatment. *JOURNAL OF CONTROLLED RELEASE* **2023**, *361*, 130-146. DOI: 10.1016/j.jconrel.2023.07.054.

(44) Mu, Q.; Yu, J.; Griffin, J.; Wu, Y.; Zhu, L.; McConnachie, L.; Ho, R. Novel drug combination nanoparticles exhibit enhanced plasma exposure and doseresponsive effects on eliminating breast cancer lung metastasis. *PLOS ONE* **2020**, *15* (3). DOI: 10.1371/journal.pone.0228557.

(45) Murray, S.; Briasoulis, E.; Linardou, H.; Bafaloukos, D.; Papadimitriou, C. Taxane resistance in breast cancer: Mechanisms, predictive biomarkers and circumvention strategies. *CANCER TREATMENT REVIEWS* **2012**, *38* (7), 890-903. DOI: 10.1016/j.ctrv.2012.02.011.

(46) Patel, P.; Fetse, J.; Lin, C.; Guo, Y.; Hasan, M.; Nakhjiri, M.; Zhao, Z.; Jain, A.; Cheng, K. Development of amino acid-modified biodegradable lipid nanoparticles for siRNA delivery. *ACTA BIOMATERIALIA* **2022**, *154*, 374-384. DOI: 10.1016/j.actbio.2022.09.065.

(47) Peng, W.; Chen, J.; Liu, C.; Malu, S.; Creasy, C.; Tetzlaff, M.; Xu, C.; McKenzie, J.; Zhang, C.; Liang, X.; et al. Loss of PTEN Promotes Resistance to T Cell-Mediated Immunotherapy. *CANCER DISCOVERY* **2016**, *6* (2), 202-216. DOI: 10.1158/2159-8290.CD-15-0283.

(48) Perazzolo, S.; Shireman, L.; McConnachie, L.; Koehn, J.; Kinman, L.; Lee, W.; Lane, S.; Collier, A.; Shen, D.; Ho, R. Integration of Computational and Experimental Approaches to Elucidate Mechanisms of First -Pass Lymphatic Drug Sequestration and Long -Acting Pharmacokinetics of the Injectable Triple -HIV Drug Combination TLC -ART 101. *JOURNAL OF PHARMACEUTICAL SCIENCES* **2020**, *109* (5), 1789-1801.

(49) Patel, P.; Tonog, P. A. D. L. *Normal Saline*; StatPearls, 2025.

(50) Puluhulawa, L.; Joni, I.; Elamin, K.; Mohammed, A.; Muchtaridi, M.; Wathoni, N. Chitosan-Hyaluronic Acid Nanoparticles for Active Targeting in Cancer Therapy. *POLYMERS* **2022**, *14* (16). DOI: 10.3390/polym14163410.

(51) Raab, M.; Kostova, I.; Pena-Llopis, S.; Fietz, D.; Kressin, M.; Aberoumandi, S.; Ullrich, E.; Becker, S.; Sanhaji, M.; Strebhardt, K. Rescue of p53 functions by in vitro-transcribed mRNA impedes the growth of high-grade serous ovarian cancer. *CANCER COMMUNICATIONS* **2024**, *44* (1), 101-126. DOI: 10.1002/cac2.12511.

(52) Ramakrishnan, R.; Assudani, D.; Nagaraj, S.; Hunter, T.; Cho, H.; Antonia, S.; Altiok, S.; Celis, E.; Gabrilovich, D. Chemotherapy enhances tumor cell susceptibility to CTL-mediated killing during cancer immunotherapy in mice. *JOURNAL OF CLINICAL INVESTIGATION* **2010**, *120* (4), 1111-1124. DOI: 10.1172/JCI40269.

(53) Ramakrishnan, R.; Gabrilovich, D. Mechanism of synergistic effect of chemotherapy and immunotherapy of cancer. *CANCER IMMUNOLOGY IMMUNOTHERAPY* **2011**, *60* (3), 419-423, Review. DOI: 10.1007/s00262-010-0930-1.

(54) Rampersad, S. Multiple Applications of Alamar Blue as an Indicator of Metabolic Function and Cellular Health in Cell Viability Bioassays. *SENSORS* **2012**, *12* (9), 12347-12360. DOI: 10.3390/s120912347.

(55) Raza, M.; Kumar, N.; Nair, U.; Luthra, G.; Bhattacharyya, U.; Jayasundar, S.; Jayasundar, R.; Sehrawat, S. Current updates on precision therapy for breast cancer associated brain metastasis: Emphasis on combination therapy. *MOLARECULAR AND CELLULAR BIOCHEMISTRY* **2021**, *476* (9), 3271-3284, Review. DOI: 10.1007/s11010-021-04149-7.

(56) Restifo, N.; Marincola, F.; Kawakami, Y.; Taubenberger, J.; Yannelli, J.; Rosenberg, S. Loss of functional beta(2)-microglobulin in metastatic melanomas from five patients receiving immunotherapy. *JOURNAL OF THE NATIONAL CANCER INSTITUTE* **1996**, *88* (2), 100-108. DOI: 10.1093/jnci/88.2.100.

(57) Schmid, P.; Chui, S.; Emens, L. Atezolizumab and Nab-Paclitaxel in Advanced Triple-Negative Breast Cancer REPLY. *NEW ENGLAND JOURNAL OF MEDICINE* **2019**, *380* (10), 987-988.

(58) Schoenfeld, A.; Hellmann, M. Acquired Resistance to Immune Checkpoint Inhibitors. *CANCER CELL* **2020**, *37* (4), 443-455. DOI: 10.1016/j.ccell.2020.03.017.

(59) Shaabani, E.; Sharifiaghdam, M.; De Keersmaecker, H.; De Rycke, R.; De Smedt, S.; Faridi-Majidi, R.; Braeckmans, K.; Fraire, J. Layer by Layer Assembled Chitosan-Coated Gold Nanoparticles for Enhanced siRNA Delivery and Silencing. *INTERNATIONAL JOURNAL OF MOLARECULAR SCIENCES* **2021**, *22* (2). DOI: 10.3390/ijms22020831.

(60) Siegel, R.; Kratzer, T.; Giaquinto, A.; Sung, H.; Jemal, A. Cancer statistics, 2025. *CA-A CANCER JOURNAL FOR CLINICIANS* **2025**, *75* (1), 10-45. DOI: 10.3322/caac.21871.

(61) Singha, K.; Namgung, R.; Kim, W. Polymers in Small-Interfering RNA Delivery. *NUCLEIC ACID THERAPEUTICS* **2011**, *21* (3), 133-147. DOI: 10.1089/nat.2011.0293.

(62) Skinner, K.; Haiderali, A.; Huang, M.; Schwartzberg, L. Real-world effectiveness outcomes in patients diagnosed with metastatic triple-negative breast cancer. *FUTURE ONCOLOGY* **2021**, *17* (8), 931-942. DOI: 10.2217/fon-2020-1021.

(63) Stratton, M.; Campbell, P.; Futreal, P. The cancer genome. *NATURE* **2009**, *458* (7239), 719-724. DOI: 10.1038/nature07943.

(64) Szewczyk-Roszczenko, O.; Barlev, N. The Role of p53 in Nanoparticle-Based Therapy for Cancer. *CELLS* **2023**, *12* (24). DOI: 10.3390/cells12242803.

(65) Tamargo, J.; Le Heuzey, J.; Mabo, P. Narrow therapeutic index drugs: a clinical pharmacological consideration to flecainide. *EUROPEAN JOURNAL OF CLINICAL PHARMACOLOGY* **2015**, *71* (5), 549-567. DOI: 10.1007/s00228-015-1832-0.

(66) Thorek, D.; Tsourkas, A. Size, charge and concentration dependent uptake of iron oxide particles by non-phagocytic cells. *BIOMATERIALS* **2008**, *29* (26), 3583-3590. DOI: 10.1016/j.biomaterials.2008.05.015.

(67) Vagia, E.; Mahalingam, D.; Cristofanilli, M. The Landscape of Targeted Therapies in TNBC. *CANCERS* **2020**, *12* (4). DOI: 10.3390/cancers12040916.

(68) van den Bent, M.; van Putten, W.; Hilkens, P.; de Wit, R.; van der Burg, M. Retreatment with dose-dense weekly cisplatin after previous cisplatin chemotherapy is not complicated by significant neuro-toxicity. *EUROPEAN JOURNAL OF CANCER* **2002**, *38* (3), 387-391.

(69) Villanueva, A.; Cañete, M.; Roca, A.; Calero, M.; Veintemillas-Verdaguer, S.; Serna, C.; Morales, M.; Miranda, R. The influence of surface functionalization on the enhanced internalization of magnetic nanoparticles in cancer cells. *NANOTECHNOLOGY* **2009**, *20* (11). DOI: 10.1088/0957-4484/20/11/115103.

(70) Waks, A.; Winer, E. Breast Cancer Treatment A Review. *JAMA-JOURNAL OF THE AMERICAN MEDICAL ASSOCIATION* **2019**, *321* (3), 288-300, Review. DOI: 10.1001/jama.2018.19323.

(71) Weng, Y.; Li, C.; Yang, T.; Hu, B.; Zhang, M.; Guo, S.; Xiao, H.; Liang, X.; Huang, Y. The challenge and prospect of mRNA therapeutics landscape. *BIOTECHNOLOGY ADVANCES* **2020**, *40*. DOI: 10.1016/j.biotechadv.2020.107534.

(72) Xu, B.; Xia, S.; Wang, F.; Jin, Q.; Yui, T.; He, L.; Chen, Y.; Liu, Y.; Li, S.; Tan, X.; et al. Polymeric Nanomedicine for Combined Gene/Chemotherapy Elicits Enhanced Tumor Suppression. *MOLARECULAR PHARMACEUTICS* **2016**, *13* (2), 663-676. DOI: 10.1021/acs.molarpharmaceut.5b00922.

(73) Yin, L.; Duan, J.; Bian, X.; Yu, S. Triple-negative breast cancer molarecular subtyping and treatment progress. *BREAST CANCER RESEARCH* **2020**, *22* (1). DOI: 10.1186/s13058-020-01296-5.

(74) Young, L.; Searle, P.; Onion, D.; Mautner, V. Viral gene therapy strategies: from basic science to clinical application. *JOURNAL OF PATHOLOGY* **2006**, *208* (2), 299-318. DOI: 10.1002/path.1896.

(75) Yu, J.; Xu, X.; Griffin, J.; Mu, Q.; Ho, R. Drug Combination Nanoparticles Containing Gemcitabine and Paclitaxel Enable Orthotopic 4T1 Breast Tumor Regression. *CANCERS* **2024**, *16* (16). DOI: 10.3390/cancers16162792.

(76) Yu, J.; Mu, Q.; Perazzolo, S.; Griffin, J.; Zhu, L.; McConnachie, L.; Shen, D.; Ho, R. Novel Long-Acting Drug Combination Nanoparticles Composed of Gemcitabine and Paclitaxel Enhance Localization of Both Drugs in Metastatic Breast Cancer Nodules. *PHARMACEUTICAL RESEARCH* **2020**, *37* (10). DOI: 10.1007/s11095-020-02888-8.

(77) Zaretsky, J.; Garcia-Diaz, A.; Shin, D.; Escuin-Ordinas, H.; Hugo, W.; Hu-Lieskovan, S.; Torrejon, D.; Abril-Rodriguez, G.; Sandoval, S.; Barthly, L.; et al. Mutations Associated with Acquired Resistance to PD-1 Blockade in Melanoma. *NEW ENGLAND JOURNAL OF MEDICINE* **2016**, *375* (9), 819-829. DOI: 10.1056/NEJMoa1604958.

(78) Zhang, C.; Zhao, Y.; Zhang, E.; Jiang, M.; Zhi, D.; Chen, H.; Cui, S.; Zhen, Y.; Cui, J.; Zhang, S. Co-delivery of paclitaxel and anti-VEGF siRNA by tripeptide lipid nanoparticle to enhance the anti-tumor activity for lung cancer therapy. *DRUG DELIVERY* **2020**, *27* (1), 1397-1411. DOI: 10.1080/10717544.2020.1827085.

(79) Zhang, C.; Zhang, X.; Zhao, W.; Zeng, C.; Li, W.; Li, B.; Luo, X.; Li, J.; Jiang, J.; Deng, B.; et al. Chemotherapy drugs derived nanoparticles encapsulating mRNA encoding tumor suppressor proteins to treat triple-negative breast cancer. *NANO RESEARCH* **2019**, *12* (4), 855-861. DOI: 10.1007/s12274-019-2308-9.

(80) Zhang, P.; Yin, Y.; Mo, H.; Zhang, B.; Wang, X.; Li, Q.; Yuan, P.; Wang, J.; Zheng, S.; Cai, R.; et al. Better pathologic complete response and relapse-free survival after carboplatin plus paclitaxel compared with epirubicin plus paclitaxel as neoadjuvant chemotherapy for locally advanced triple-negative breast cancer: a randomized phase 2 trial. *ONCOTARGET* **2016**, *7* (37), 60647-60656. DOI: 10.18632/oncotarget.10607.